Mon. Not. R. Astron. Soc. **000**, 1–8 (2010) Printed 31 March 2010 (MN LATEX style file v2.2)

# The Structure of Molecular Clouds: II - Column Density and Mass Distributions

Dirk Froebrich [1⋆] Jonathan Rowles [1†]
[1]*Centre for Astrophysics & Planetary Science, The University of Kent, Canterbury, Kent CT2 7NH, U.K.*

Accepted ..... Received ..... ; in original form .....

**ABSTRACT**

The formation of stars is inextricably linked to the structure of their parental molecular clouds. Here we take a number of nearby giant molecular clouds (GMCs) and analyse their column density and mass distributions. This investigation is based on four new all-sky median colour excess extinction maps determined from 2MASS. The four maps span a range of spatial resolution of a factor of eight. This allows us to determine cloud properties at a common spatial scale of 0.1 pc, as well as to study the scale dependence of the cloud properties.

We find that the low column density and turbulence dominated part of the clouds can be well fit by a log-normal distribution. However, above a universal extinction threshold of $6.0 \pm 1.5$ mag $A_V$ there is excess material compared to the log-normal distribution in all investigated clouds. This material represents the part of the cloud that is currently involved in star formation, and thus dominated by gravity. Its contribution to the total mass of the clouds ranges over two orders of magnitude from 0.1 to 10 %. This implies that our clouds sample various stages in the evolution of GMCs. Furthermore, we find that the column density and mass distributions are extremely similar between clouds if we analyse only the high extinction material. On the other hand, there are significant differences between the distributions if only the low extinction, turbulence dominated regions are considered. This shows that the turbulent properties differ between clouds depending on their environment. However, no significant influence on the predominant mode of star formation (clustered or isolated) could be found. Furthermore, the fraction of the cloud actively involved in star formation is only governed by gravity, with the column density and mass distributions not significantly altered by local feedback processes.

**Key words:** Stars: formation – ISM: dust, extinction – ISM: clouds – ISM: structure

## 1 INTRODUCTION

The study of Giant Molecular Clouds (GMCs) is of great importance to understand star formation. Their properties (density distribution, dynamics, temperature, etc.) are thought to be vital in determining whether, where and how stars are forming within them. Turbulent motions inside a cloud cause fragmentation and hence determine the density distribution (Padoan et al. (1997), Ballesteros-Paredes et al. (1999)). This in turn should have an influence on which mode of star formation (isolated or clustered) is occurring (Klessen, Heitch and Mac Low (2000)). It is, however, unclear if this is the sole determinant of the star formation mode. Or are there other important causes such as the environment, feedback and/or magnetic fields?

One way to try to answer these questions is to investigate the column density structure of a large number of GMCs in a systematic, comparable and unbiased fashion. This means ideally one should use the same tracer of column density for all clouds. Such a tracer should be as bias free as possible and all clouds should be investigated at the same physical spatial resolution. There are a number of techniques to determine the column density of clouds. These include molecular line emission, dust continuum emission, scattered infrared light or extinction measurements. The latter on the bases of star counts, colour excess or combined methods. See Froebrich & Rowles (2010) for a brief summary and discussion of the advantages and disadvantages of the various techniques. It has been shown by Goodman et al. (2008) that near infrared extinction mapping is the best tracer of the 'real' column density of a cloud, based only on the assumption of a constant gas to dust ratio.

A number of large scale maps of the column density distribution of clouds have been made to date, which could be used to compare the structure of a number of GMCs. These are for example the maps by Cambrésy (1999), Schlegel et al. (1998), Dobashi et al. (2005), Froebrich et al. (2007) and Rowles and Froebrich (2009). Some of them do not use the ideal tracer (extinction) for the col-

⋆ E-mail: df@star.kent.ac.uk,
† E-mail: jr262@kent.ac.uk

**Table 1.** Summary table of the clouds analysed in this paper. We list the cloud name, the range in galactic coordinates ($l$;$b$) covered by the region and the distance (d) adopted in this paper. *The cloud Auriga 1 is referred to as the California Molecular Cloud in Lada et al. (2009). The references for the adopted distances are the following: [1] Lada et al. (2009); [2] Kenyon et al. (2008); [3] Kun (2008); [4] Knude & Hog (1998); [5] Bally et al. (1999); [6] Muench (2008); [7] Lombardi et al. (2008); [8] Carpenter (2008); [9] Motte (2001); [10] Straizys (1996).

| Name | $l$ range | $b$ range | d [pc] |
|---|---|---|---|
| Auriga 1* | 156° – 173° | −12.0° – −3.0° | 450± 23[1] |
| Auriga 2 | 175° – 186° | −11.0° – −2.0° | 140± 28[2] |
| Cepheus | 100° – 120° | +5.0° – +20.0° | 390±125[3] |
| Chamaeleon | 296° – 304° | −18.0° – −13.0° | 150± 30[4] |
| Circinus | 316° – 319° | −6.0° – −3.0° | 700±350[5] |
| Corona Australis | 359° – 1° | −20.0° – −17.0° | 170± 34[4] |
| $\lambda$-Ori | 188° – 201° | −18.0° – −6.0° | 400± 80[6] |
| Lupus 1, 2 | 334° – 342° | +11.0° – +19.0° | 155± 8[7] |
| Lupus 3, 4, 5, 6 | 335° – 344° | +5.0° – +11.0° | 155± 8[7] |
| Monoceros | 212° – 222° | −13.0° – −7.0° | 830± 50[8] |
| Ophiuchus | 350° – 360° | +12.0° – +19.0° | 119± 6[7] |
| Orion A | 208° – 219° | −21.0° – −16.0° | 410± 80[6] |
| Orion B | 201° – 211° | −17.0° – −8.0° | 410± 80[6] |
| Perseus | 156° – 163° | −25.0° – −15.0° | 310± 65[9] |
| Serpens | 30° – 32° | +4.0° – +6.0° | 260± 10[10] |
| Taurus | 164° – 178° | −19.0° – −10.0° | 140± 28[2] |

umn density. Others use star counts, which result in a distance dependent bias in the column density distribution (Froebrich & del Burgo (2006)), similar to using the mean colour excess instead of the median. One bias they all have in common is that clouds at different distances are mapped at different spatial resolutions. This will naturally lead to a change in the observed column density distribution, since for more distant clouds one averages over larger physical scales. This will lead to the effect that small scale high extinction regions are averaged out and the column density distributions are skewed. In order to compare the structure of GMCs with each other, one has to determine the column density distribution at similar physical scales and using the same 'good' tracer for all investigated clouds.

Only then can we attempt to draw conclusions about similarities and differences in their structures. This can be done by analysing the column density and mass distribution (the focus of this paper) or determining structure functions (the focus of the next paper in the series) and comparing it to model predictions such as published by Kolmogorov (1941), She & Leveque (1994) and Boldyrev (2002). In our previous paper (Rowles & Froebrich (2009), Paper I hereafter) we presented all-sky extinction maps determined using data from 2MASS (Skrutskie et al. (2006)). These were created using an adaptation of the NICE method (Lada et al. (1994)), median colour excess determination and variable spatial resolution to obtain a constant signal to noise ratio. Here we present and analyse additional maps, determined using a range of constant spatial resolutions to map different clouds at similar spatial scales.

In Sect. 2 we briefly describe the new maps created for the project, and explain the data analysis methods. In Sect. 3 we present the results for our selection of nearby GMCs. We discuss these results and draw conclusions in Sect. 4.

## 2 DATA ANALYSIS

### 2.1 Cloud selection

For our analyses we selected a number of nearby GMCs. Since we are interested in their column density distribution, we selected only clouds that are not situated directly in the Galactic Plane. This avoids that there are two clouds along the same line of sight, rendering the column density analysis difficult. Furthermore, only sufficiently large (or nearby) clouds are selected. This ensures that we have enough area (pixels) in our maps to analyse the column density distribution. Finally, only GMCs with a well known distance are included in our investigations. This selection process leaves 16 cloud complexes. Their names, coordinate ranges, distances and references are listed in Table 1. To allow a comparison to the earlier work by Froebrich et al. (2007) we adopt the names for the regions from this paper. In the case of the Lupus complex, we treat several of the small clouds as one, in order to have enough area to be analysed. One should hence keep in mind when interpreting this data that they are composed of several clouds.

### 2.2 Constant resolution extinction maps

The determination of the new constant resolution extinction maps has been performed in exactly the same way as described in Paper I. We determine median $\langle J-H\rangle$ and $\langle H-K\rangle$ colour excess maps, with the same position dependent zero point as in Paper I. These maps are converted into optical extinction maps and are averaged (following Eq. 1 and using $\beta = 1.7$ as in Paper I). Similarly, maps of the uncertainties are calculated. Already in Paper I one constant resolution map has been determined. There the spatial resolution changed from $0.5'$ to $2.0'$, depending on the galactic latitude. Only stars within this radius were included in the extinction determination. In contrast to this, the new maps consist of square shaped pixels with no oversampling. In other words, the pixel values in those maps are completely independent on the neighbouring pixels.

$$A_V = \frac{5.689}{2} \cdot \left( \frac{\langle J-H\rangle}{\left(\frac{\lambda_H}{\lambda_J}\right)^{\beta} - 1} + \frac{\langle H-K\rangle}{1 - \left(\frac{\lambda_K}{\lambda_H}\right)^{-\beta}} \right) \qquad (1)$$

For the purpose of this paper, we have calculated a number of further constant spatial resolution maps, in total four, with a different resolution. We used the resolution of the maps in Paper I for the first map, and then increased the pixel size in steps of a factor of two. This ensures we have an extinction map of each cloud with spatial resolutions covering almost an order of magnitude. Since the range of distances for our clouds varies by less than that, there will be one common physical spatial resolution where each cloud has been observed.

The new all-sky extinction maps available are listed in Table 2. They are labeled maps 1 through 4 depending on the pixel sizes used. Note the dependence of the actual pixel size of each map with galactic latitude.

### 2.3 Cloud structure analysis

We can now determine the column density distribution for each cloud at four different spatial scales. As a first step we extract the extinction values for each cloud from the maps 1 to 4. We then plot histograms of the number of pixels with a given extinction value,

**Table 2.** Pixel sizes of the new all-sky constant resolution extinction maps.

| $\|b\|$ range | Pixel size Map 1 [′] | Pixel size Map 2 [′] | Pixel size Map 3 [′] | Pixel size Map 4 [′] |
|---|---|---|---|---|
| 90° – 50° | 2.0 | 4.0 | 8.0 | 12.0 |
| 50° – 40° | 1.5 | 3.0 | 6.0 | 12.0 |
| 40° – 20° | 1.0 | 2.0 | 4.0 | 8.0 |
| 20° – 0° | 0.5 | 1.0 | 2.0 | 4.0 |

or the integrated number of pixels above a given extinction – i.e. a measure of the mass distribution.

The width of the histograms bins was varied. We used 1/8th, 1/4th, 1/2 and 1 mag of optical extinction. All subsequent analyses were conducted for each bin size, in order to check for systematic dependence of the results on this. It turned out that, as long as there are a sufficient number of pixels in each bin, the results do not depend on the bin size. For small clouds and large spatial resolution the last bin width (1 mag) might contain not enough datapoints. We hence excluded these outliers and averaged the results obtained from the other histogram bin widths to calculate the final result.

#### *2.3.1 Log-Normal Fits to the Column Density Distribution*

The first method of analysis performed was to fit an analytic function to the column density distribution histogram showing the number of pixels $N$ with an optical extinction $A_V$. Following Lombardi et al. (2008) we fit our clouds with a log-normal distribution of the form:

$$h(A_V) = \frac{a}{A_V - A_0} \exp\left[-\frac{(\ln(A_V - A_0) - \ln A_1)^2}{2(\ln \sigma)^2}\right] \quad (2)$$

If there are only a small number of clouds along the line of sight (certainly valid due to our selection criteria of clouds; see Sect. 2.1) and the underlying density distribution is log-normal (as predicted e.g. by Vázquez-Semadeni & Garcia (2001)) a good fit should be obtained.

#### *2.3.2 The $\log(N)$ vs $A_V$ Column Density Distribution*

A plot of the optical extinction vs $\log(N)$, where $N$ is the number of pixels with the given $A_V$ value, is to a large extent linear. This is expected since the column density distribution is caused by turbulent fragmentation and turbulence is intrinsically self-similar. We can hence use the slope ($\gamma$) of this distribution to characterise the column density distribution.

For almost all clouds there are two ranges of extinction where the plot is linear. Both possess different slopes $\gamma$ and typically the change of slope happens between 5 and 10 mag of $A_V$. We hence determine for each cloud two slope values, one for the lower extinction region ($\gamma_{\rm low}$) and one for the high $A_V$ material ($\gamma_{\rm high}$). The extinction ranges where the slopes are constant are set for each cloud manually.

#### *2.3.3 The $\log(M)$ vs $A_V$ Mass Distribution*

Similar to the analysis of the column density distribution we can calculate the mass $M$ in the cloud at extinction values higher than a given $A_V$ value. In other words we integrate the extinction values above $A_V$ and convert to masses using the pixel size and distance to the cloud. Like for the investigation of the column density, this mass distribution shows, over a range of $A_V$ values, an exponential behavior. We can hence fit the slope ($\delta$) in the $\log(M)$ vs $A_V$ diagram to characterise the mass distribution.

Again, for most clouds there are two regimes with different slopes. There is the lower $A_V$ region (characterised by $\delta_{\rm low}$), whose mass distribution is governed by the turbulent properties of the cloud material. And the high $A_V$ region (characterised by $\delta_{\rm high}$), where gravity becomes important and changes the mass distribution. The extinction value where this change of behavior is observed ($A_{V,SF}$), can be seen as the extinction threshold for star formation, first described by Johnstone et al. (2004) in Ophiuchus.

## 3 RESULTS

### 3.1 Scale Dependent Effects

We are planning to compare parameters of cloud structure for different clouds. Hence, all parameters need to be determined at a physical resolution common to all investigated clouds. Since most of our clouds are reasonably nearby, we chose 0.1 pc, which corresponds to the Jeans mass of a core with a temperature of 15 K and a density of GMCs of $5 \cdot 10^4$ cm$^{-3}$.

There are in principle the following ways to determine the structure parameters at this common scale for all clouds: i) determine the extinction maps for each cloud at the appropriate spatial resolution; ii) determine the the maps for all clouds at a sufficiently high spatial resolution and rebin them to the correct resolution before performing the data analysis; iii) Determine the cloud properties at a number of spatial resolutions and interpolate them to 0.1 pc. Option i) would certainly be the most desirable, however the most laborious. Below we will show that option ii) should be performed with great care, since it can lead to erroneous results. Option iii) does not only allow us to determine the cloud properties at the common physical scale, but also to investigate the properties at other spatial resolutions.

In the left panel of Fig. 1 we show how the slope $\gamma_{\rm low}$ for the cloud Auriga 1 depends on the spatial resolution. At each spatial resolution we determine the slope four times using different histogram widths, as discussed in Sect. 2.3. As one can see, these slopes agree very well and can be averaged (solid line in the right panel of Fig. 1). For the other clouds a similar behavior is found (see Appendix A for the remaining plots). About half the clouds show no dependence of the slope on the scale and the other half a significant decrease of $\gamma_{\rm low}$ with decreasing resolution.

The general trend for Auriga 1 is that the slope $\gamma_{\rm low}$ decreases towards larger spatial scales. On can understand this trend simply by assuming that the cloud contains a number of very small, high extinction cores which are simply not picked up at the larger spatial scales. This is not the case for all clouds investigated. In some cases we find more or less constant slopes with changing spatial scale. In those clouds the fraction of very small high extinction cores is probably smaller.

We investigated what happens when we simply rebin the highest spatial resolution image to the lower resolution and we redetermine the slopes $\gamma_{\rm low}$. The results for Auriga 1 are shown in the right panel in Fig. 1 as a dotted line. One finds that the general trend of the slope values is retained. However, individual $\gamma_{\rm low}$ values in the rebinned images can differ by almost the one sigma uncertainties of the values obtained in the maps determined at the respective spatial resolution. See Appendix A1 and A2 for the effects the rebinning has on the $\gamma_{\rm low}$ and $\gamma_{\rm high}$ values. In general the

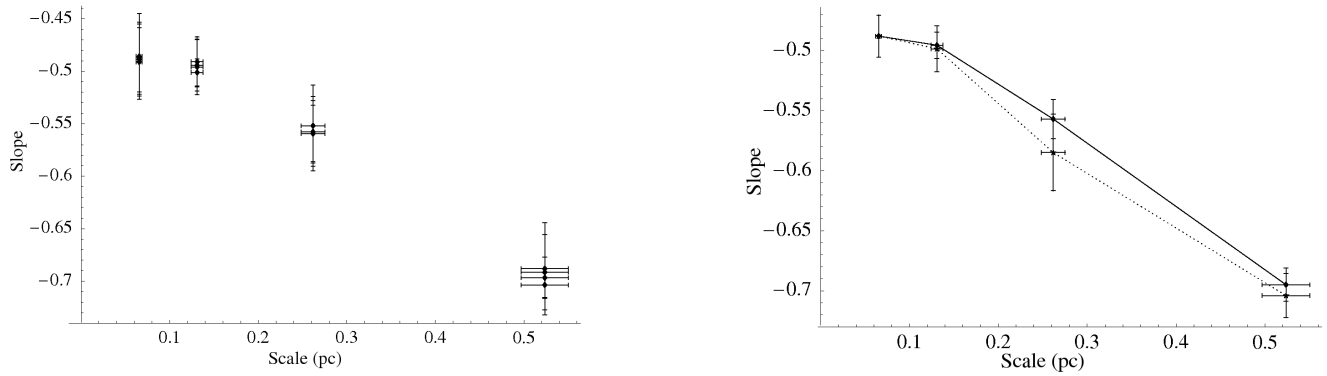


**Figure 1. Left:** A plot showing measured slopes $\gamma_{\rm low}$ against spatial scale for the Auriga 1 cloud. The four data points at each resolution correspond to the four histogram bin widths used. **Right:** The solid line shows the averaged slopes $\gamma_{\rm low}$ from the left panel. The dotted line shows the slopes $\gamma_{\rm low}$ if the highest resolution image is simply rebinned to the lower resolutions.

differences are well below the one sigma uncertainties. However, in a few cases, such as the above quoted example of Auriga 1, larger differences can be found.

As a consequence of this result we chose to perform option iii) to determine our cloud structure parameters for all clouds at 0.1 pc resolution. We calculate all parameters at each of the four spatial resolutions available to us, and then interpolate to obtain the values at 0.1 pc. All subsequent analysis is performed this way.

### 3.2 Log-Normal Fits to the Column Density Distribution

Using the technique described in Sect. 2.3.1 we obtained fit parameters for each cloud we analysed with Eq. 2. In Table 3 we summarise the fit parameters and the root mean square deviation ($rms$) values obtained for the various spatial resolutions and histogram bin sizes for the Auriga 1 cloud as an example. There is a general trend visible for all parameters. In particular the width of the distribution increases with spatial scale. This is expected, since more and more small scale high extinction cores are not detected anymore at these coarse resolutions.

In Fig. 2 we show the normalised column density distribution for the Auriga 1 cloud as a solid line (shown is the data for the spatial resolution closest to 0.1 pc). Overplotted is a fit with parameters scaled to 0.1 pc spatial scale. Similar plots for all individual clouds can be seen in the Appendix A3. We list the fit parameters and $rms$ values (scaled to 0.1 pc resolution) for all clouds in Table 4.

### 3.3 The $\log(N)$ vs $A_V$ Column Density Distribution

As described in Sect. 2.3.2 we calculate gradients $\gamma$ for each cloud in our sample. As discussed, there are usually at least two distinct regions with different slopes. One region, at low extinction values ($\gamma_{\rm low}$) characterises the general turbulence of the cloud. At higher extinction values ($\gamma_{\rm high}$) gravity becomes important and changes the column density away from a log-normal distribution. As an example we show the $\log(N)$ vs $A_V$ for Auriga 1 in Fig. 2. The plots for the other clouds are shown in Appendix A4. We also show how the slopes $\gamma_{\rm low}$ and $\gamma_{\rm high}$ depend on the spatial resolution for all clouds in Fig. 4.

The gradients for all clouds, averaged and interpolated to 0.1 pc resolution, are summarised in Table 4. In general the $\gamma_{\rm low}$ values are about twice as negative as the $\gamma_{\rm high}$ values. More importantly the scatter for the slopes in the high column density regions

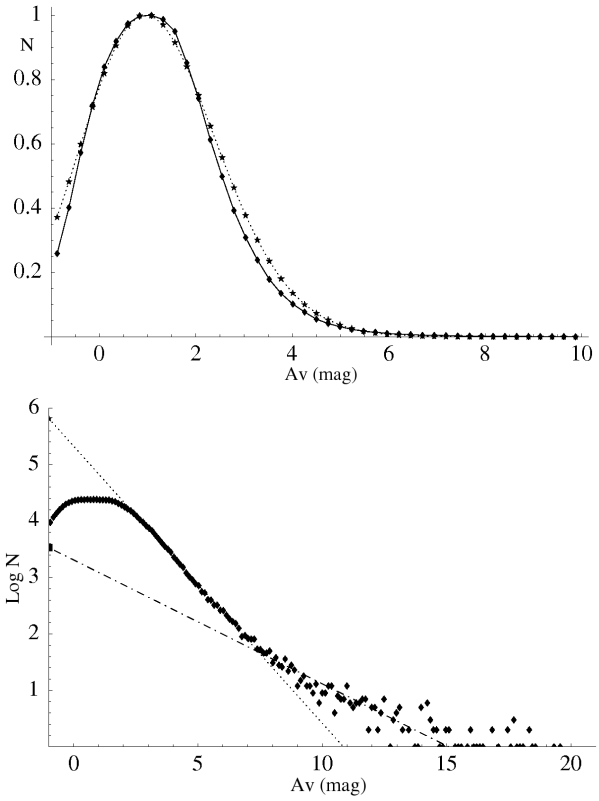


**Figure 2. Top:** Plot of the best Log-Normal fit (dotted line) to the normalised column density distribution (solid line) for the Auriga 1 cloud. The fit parameters are interpolated to a spatial scale of 0.1 pc, and the data for the spatial resolution closest to 0.1 pc are shown. **Bottom:** Plot of the $\log N$ vs $A_V$ column density distribution for the Auriga 1 cloud (symbols). Overplotted are the two fits obtained for the low and high column density region.

of the clouds is smaller than in the low $A_V$ regions. For the averages and scatter for all clouds we find: $\langle\gamma_{\rm low}\rangle = -0.45 \pm 0.15$ and $\langle\gamma_{\rm high}\rangle = -0.20 \pm 0.06$. This indicates, that once gravity becomes important enough to influence the column density distribution (i.e. star formation starts), then we will find far fewer differences between the various clouds. While at low column densities, where external factors (proximity to Supernovae, etc.) determine the turbulent motions, much larger cloud to cloud differences are seen.

**Table 3.** Fit parameters for the Auriga 1 cloud obtained for the various spatial resolutions and histogram bin sizes. We list the parameters from the fit of the log-normal distribution, as well as the slopes $\gamma$ and $\delta$.

| Sp. Res. [arcmin] | Sp. Res. [pc] | Bin size [mag] | $a$ [mag] | $A_0$ [mag] | $A_1$ [mag] | $\sigma$ [mag] | $rms$ [$\sigma$] | $\gamma_{\mathbf{low}}$ | $\gamma_{\mathbf{high}}$ | $\delta_{\mathbf{low}}$ | $\delta_{\mathbf{high}}$ |
|---|---|---|---|---|---|---|---|---|---|---|---|
| 0.5 | 0.065 | 0.125 | 26.2 | -24.2 | 25.0 | 1.06 | 6.4 | -0.49 | -0.22 | -0.38 | -0.14 |
| 0.5 | 0.065 | 0.250 | 26.9 | -24.7 | 25.6 | 1.06 | 4.7 | -0.49 | -0.23 | -0.38 | -0.14 |
| 0.5 | 0.065 | 0.500 | 31.5 | -29.2 | 30.1 | 1.05 | 3.4 | -0.49 | -0.23 | -0.38 | -0.14 |
| 0.5 | 0.065 | 1.000 | 84.6 | -80.2 | 81.0 | 1.02 | 2.0 | -0.49 | -0.22 | -0.39 | -0.14 |
| 1.0 | 0.131 | 0.125 | 11.1 | -9.8 | 10.8 | 1.12 | 8.8 | -0.50 | -0.26 | -0.36 | -0.13 |
| 1.0 | 0.131 | 0.250 | 11.2 | -9.8 | 10.9 | 1.12 | 6.5 | -0.49 | -0.27 | -0.36 | -0.13 |
| 1.0 | 0.131 | 0.500 | 11.5 | -10.1 | 11.5 | 1.12 | 4.8 | -0.49 | -0.26 | -0.37 | -0.13 |
| 1.0 | 0.131 | 1.000 | 13.2 | -11.7 | 12.8 | 1.11 | 2.9 | -0.49 | -0.25 | -0.37 | -0.13 |
| 2.0 | 0.262 | 0.125 | 4.1 | -3.2 | 4.1 | 1.23 | 12.2 | -0.56 | -0.33 | -0.36 | -0.14 |
| 2.0 | 0.262 | 0.250 | 4.1 | -3.2 | 4.2 | 1.24 | 9.0 | -0.56 | -0.32 | -0.37 | -0.14 |
| 2.0 | 0.262 | 0.500 | 4.2 | -3.4 | 4.3 | 1.23 | 6.6 | -0.56 | -0.32 | -0.38 | -0.14 |
| 2.0 | 0.262 | 1.000 | 5.5 | -4.1 | 5.0 | 1.20 | 4.2 | -0.55 | -0.32 | -0.39 | -0.14 |
| 4.0 | 0.524 | 0.125 | 2.2 | -1.5 | 2.3 | 1.32 | 16.0 | -0.69 | -0.45 | -0.47 | -0.27 |
| 4.0 | 0.524 | 0.250 | 2.2 | -1.6 | 2.3 | 1.32 | 11.6 | -0.69 | -0.38 | -0.48 | -0.27 |
| 4.0 | 0.524 | 0.500 | 2.5 | -1.8 | 2.5 | 1.29 | 9.3 | -0.70 | -0.41 | -0.48 | -0.28 |
| 4.0 | 0.524 | 1.000 | 3.4 | -2.5 | 3.3 | 1.24 | 4.9 | -0.70 | -0.39 | -0.47 | -0.29 |

**Table 4.** Table of parameters of best fit for all clouds, at a scale of 0.1 pc. We list the parameters from the fit of the log-normal distribution, the slopes $\gamma$ and $\delta$, as well as the cloud masses, star formation threshold, extinction of a Jeans Mass core and the mass fraction of clouds involved in star formation (MSF)

| Name | $a$ [mag] | $A_0$ [mag] | $A_1$ [mag] | $\sigma$ [mag] | $rms$ [$\sigma$] | $\gamma_{\rm low}$ | $\gamma_{\rm high}$ | $\delta_{\rm low}$ | $\delta_{\rm high}$ | $M_{\rm 1mag}$ [$10^3 M_\odot$] | $A_{V,SF}$ [mag] | $A_{V,M_\odot}$ [mag] | $MSF$ [%] |
|---|---|---|---|---|---|---|---|---|---|---|---|---|---|
| Auriga 1 | 15.9 | -14.2 | 15.3 | 1.10 | 4.7 | -0.48 | -0.24 | -0.36 | -0.13 | 268 | 7.4 | 32 | 0.19 |
| Auriga 2 | 5.5 | -4.6 | 5.6 | 1.14 | 2.5 | -0.71 | -0.32 | -0.51 | -0.21 | 13 | 4.9 | 15 | 0.33 |
| Cepheus | 32.9 | -31.8 | 32.8 | 1.04 | 9.0 | -0.50 | -0.23 | -0.37 | -0.15 | 256 | 6.7 | 29 | 0.26 |
| Chamaeleon | 3.3 | -2.7 | 3.4 | 1.27 | 3.2 | -0.39 | -0.18 | -0.25 | -0.13 | 45 | 7.3 | 24 | 0.81 |
| Circinus | 9.8 | -7.5 | 9.9 | 1.17 | 4.5 | -0.36 | -0.17 | -0.24 | -0.16 | 113 | 6.8 | 30 | 1.4 |
| Corona Australis | 2.2 | -1.7 | 2.5 | 1.46 | 1.6 | -0.40 | -0.16 | -0.20 | -0.15 | 1 | 3.7 | 23 | 9.6 |
| $\lambda$-Ori | 12.8 | -12.3 | 12.9 | 1.11 | 4.6 | -0.51 | -0.34 | -0.40 | -0.13 | 122 | 7.2 | 28 | 0.12 |
| Lupus 1, 2 | 8.0 | -7.4 | 8.0 | 1.08 | 3.4 | -0.73 | -0.20 | -0.47 | -0.13 | 4.6 | 3.4 | 23 | 2.4 |
| Lupus 3, 4, 5, 6 | 4.2 | -2.7 | 4.3 | 1.22 | 2.0 | -0.73 | -0.21 | -0.47 | -0.12 | 24 | 5.1 | 25 | 0.40 |
| Monoceros | 12.5 | -11.9 | 12.6 | 1.11 | 6.7 | -0.42 | -0.18 | -0.32 | -0.12 | 74 | 4.8 | 35 | 2.0 |
| Ophiuchus | 1.5 | -0.3 | 1.5 | 1.48 | 7.0 | -0.27 | -0.11 | -0.21 | -0.13 | 9.3 | 8.6 | 27 | 0.78 |
| Orion A | 3.9 | -3.0 | 4.1 | 1.39 | 4.2 | -0.28 | -0.15 | -0.19 | -0.12 | 44 | 5.4 | 37 | 5.0 |
| Orion B | 6.4 | -5.5 | 6.5 | 1.23 | 4.3 | -0.39 | -0.13 | -0.26 | -0.11 | 78 | 6.8 | 38 | 1.1 |
| Perseus | 5.8 | -5.0 | 5.9 | 1.23 | 3.8 | -0.42 | -0.22 | -0.28 | -0.17 | 29 | 4.8 | 25 | 3.0 |
| Serpens | 12.3 | -7.3 | 12.4 | 1.13 | 2.1 | -0.32 | -0.16 | -0.21 | -0.14 | 18 | 7.7 | 31 | 1.3 |
| Taurus | 4.5 | -3.8 | 4.6 | 1.26 | 3.2 | -0.34 | -0.15 | -0.24 | -0.14 | 19 | 4.4 | 28 | 4.8 |

### 3.4 The $\log(M)$ vs $A_V$ Mass Distribution

As for the column density distribution we determine the slopes $\delta$ of the $\log(M)$ vs $A_V$ mass distribution for low and high column densities. We show as an example the mass distribution of the Auriga 1 cloud in Fig. 3. Overplotted are the linear fits. The values for all slopes $\delta$ for different spatial resolutions are listed in Table 3.

The slopes for all clouds averaged and interpolated to 0.1 pc are summarised in Table 4, the mass distributions are shown in Appendix A5. As for the values of $\gamma$, the scatter of the slopes differs for the low and high column density material. For the averages of all clouds we find: $\langle\delta_{\rm low}\rangle = -0.21 \pm 0.11$ and $\langle\delta_{\rm high}\rangle = -0.14 \pm 0.025$. Again, we find that the star forming (high column density) parts of the clouds are very similar, while the low $A_V$ (turbulence dominated) regions show a larger scatter. We show how the slopes $\delta_{\rm low}$ and $\delta_{\rm high}$ depend on the spatial resolution for all clouds in Fig. 4.

We extrapolate the fit to the low $A_V$ regions, which leads to the total mass of the cloud. For the purpose of this paper, we calculate the mass in the cloud at a column density of above 1 mag of optical extinction ($M_{\rm 1mag}$). This ensures we do not include noise and also only integrate over material that is above the threshold for self-shielding from UV radiation and molecular hydrogen formation (Hartmann et al. (2001)). Extrapolating the high $A_V$ fit towards one solar mass, one can find the extinction value a core with the Jeans Mass would have ($A_{V,M_\odot}$). Hence, this characterises the maximum extinction in the cloud before collapse starts. Furthermore, we determine the intercept between the low and high $A_V$ region, to characterise above which column density ($A_{V,SF}$) material is more likely involved in star formation than being characterised by the turbulence in the cloud. This can be seen as the star formation threshold, i.e. the column density above which star formation occurs in the cloud. Finally, the ratio of the mass in the cloud above an extinction $A_{V,SF}$ (the mass currently associated with star formation) to the total mass of the cloud above 1 mag $A_V$ is determined. Assuming that about 1/3 of the total mass associated with star formation is transformed into stars (Alves et al. (2007)) we can estimate the overall fraction of mass involved in star formation ($MSF$) an indicator of the star formation efficiency. All these values for each cloud are summarised in Table 4.

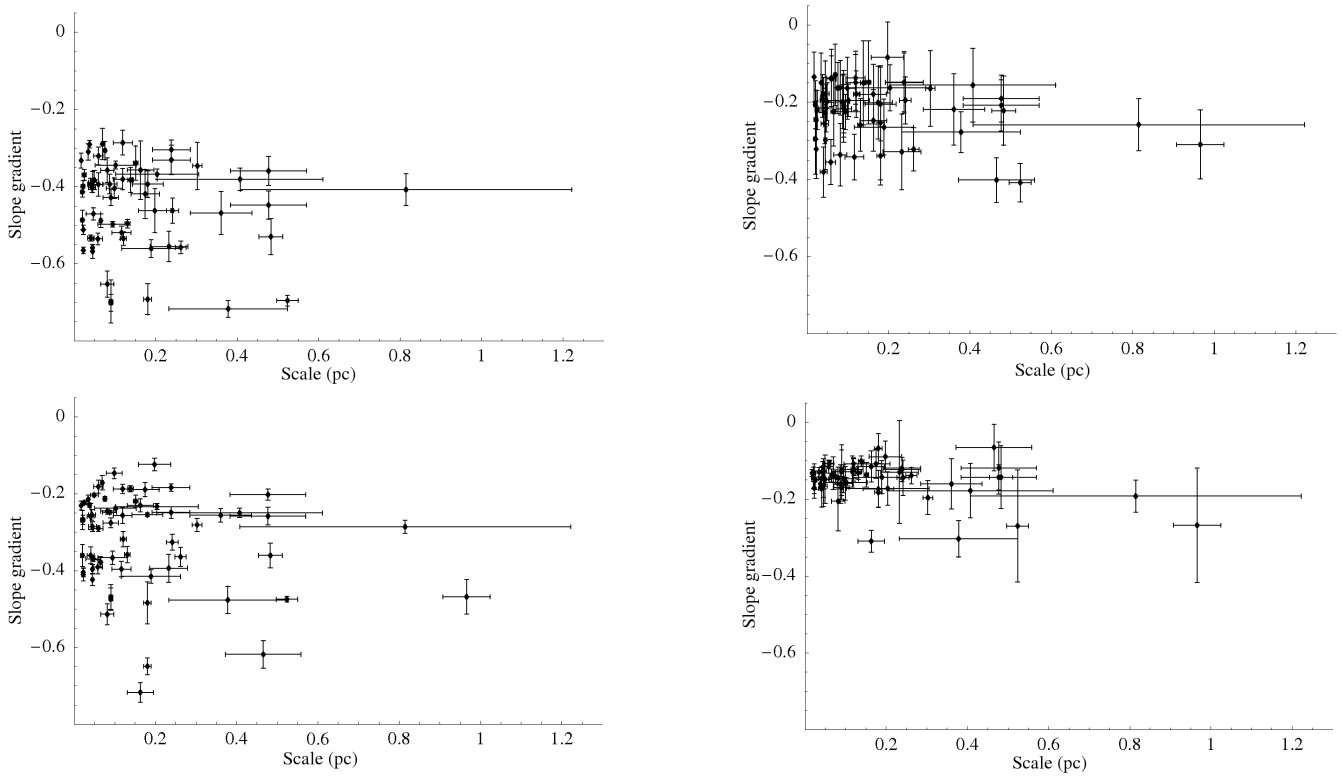


**Figure 4. Top Left:** A plot showing measured slope gradients $\gamma_{\rm low}$ against scale for all the clouds studied. **Top Right:** As in the top left panel but for the high $A_V$ region. **Bottom panels:** As in the top panels but for the slope gradients $\delta$ of the mass distribution in the clouds. All plots are shown to the same scale to show the differences in the scatter.

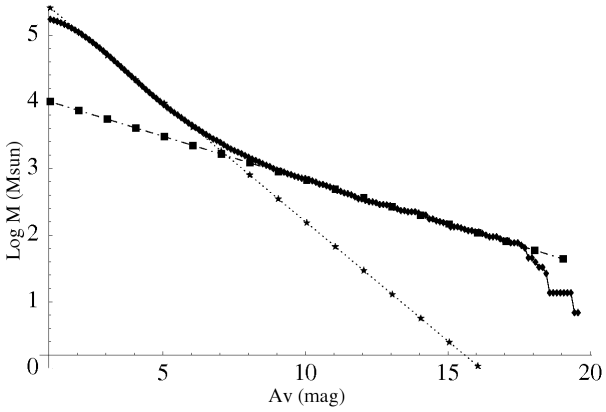


**Figure 3.** Plot of the mass distribution in the cloud Auriga 1 together with the two fits to the low and high column density regime.

## 4 DISCUSSION AND CONCLUSIONS

We investigated the column density and mass distribution of a number of GMCs based on near infrared median colour excess extinction maps determined from 2MASS. Our multi scale extinction mapping approach enabled us to determine the cloud properties homogeneously at a common scale of 0.1 pc for all clouds. Furthermore, it allowed us to investigate how the cloud properties depend on the spatial scale.

We find that for about half the investigated clouds the slope of the column density and mass distribution changes to more negative (steeper) values with increasing spatial scale. For the other half no change is found over a scale range of almost an order of magnitude. The former can be understood by the fact that at larger scales, small scale high extinction cores are not detected anymore, naturally leading to a steeper mass and column density distribution. In the latter case this does not happen. This could mean that there are no small scale high extinction regions. But this does not seem plausible, in particular since the clouds in this group are e.g. Taurus, Perseus, Ophiuchus and Orion. Another possibility is that there is no significant structure in those clouds at the smallest scales, and hence no change over the observed range of scales. We will analyse this in more detail in a forthcoming paper where we will determine the structure functions of all clouds.

Our fits to the column density distributions using a log-normal function resulted in variable outcomes. Some clouds, in particular Auriga 2, Corona Australis, Lupus 3, 4, 5, 6 and Serpens can be fit very well ($rms$ lower than $3\,\sigma$). Other clouds (Cepheus, Monoceros, Ophiuchus) cannot be fit properly by a log-normal function. This is in agreement with earlier works on some of these clouds e.g. by Lombardi et al. (2008) and more recently by Kainulainen et al. (2009). All investigated clouds show an excess of column density compared to a log-normal distribution at higher $A_V$ values. The quality of the fit is hence a measure of how much excess there is in a particular cloud. This excess material has decoupled from the general turbulent field and is dominated by gravity, in other words more likely actively involved in star formation. However, in our sample we could not find any significant correlations of the achieved quality of the log-normal fit with other cloud properties or the amount of young stars in the cloud.

The analysis of the mass distribution enables us to draw further conclusions about the structure of the clouds and their star for-

mation properties. For all clouds the change in the slope of the mass distribution is more pronounced than in the column density distribution. It is hence easier to determine the threshold at which gravity becomes the dominant force in shaping the structure. This value ranges from 3.4 mag in Lupus 1, 2 to 8.6 mag of optical extinction in Ophiuchus. We associate this with the extinction threshold for star formation, originally found to be about 7 mag of $A_V$ in Ophiuchus by Johnstone et al. (2004), in agreement with our value. On average for all clouds we find $\langle A_{\rm V,SF} \rangle = 6.0 \pm 1.5$ mag optical extinction, a rather small range.

In contrast, the mass fraction of each cloud which is currently involved in star formation varies by almost two orders of magnitude. It ranges from 0.12 % in $\lambda$-Ori to almost 10 % in Corona Australis. We note that these values are not an estimate of the star formation efficiency in these clouds. They rather should be seen as the potential of the cloud to form new stars in the next few $10^6$ yrs. The wide range of values indicates that our sample contains clouds at different stages in their evolution. We see clouds that currently only form a small number of stars (e.g. Auriga 1 and Corona Australis) but with a completely different fraction of mass involved in star formation. In Auriga 1 only a small fraction of the total material seems to be available for future star formation. On the contrary in Corona Australis a much larger fraction of material is expected to be forming stars. While other regions that currently form stars (Orion, Taurus, Perseus) still possess a significant fraction of material in a state which is expected to continue star formation. One example for a cloud which might have reached the end of star formation seems to be Ophiuchus. It is currently forming a large number of stars, but has only less than one percent of material in a gravity dominated form.

We have searched amongst our determined cloud properties for further correlations. In particular we hoped to find a link between the predominant mode of star formation in the cloud (clustered vs. isolated) with one or several cloud properties. No such correlation could be found. This is partly expected since our extinction maps show only how much material is potentially involved in star formation, and not how much gas and dust (and its properties) have lead to the star formation mode we currently see in these clouds. One could expect that the properties of the turbulence dominated part of the clouds (out of which the denser parts are formed) show some dependence on the star formation mode. Either because different turbulent properties cause different modes of star formation, or that feedback from young star clusters and isolated YSOs causes different turbulent properties. But again, no such dependence could be found in our data.

However, there are clear differences in the properties of the clouds at low column densities compared to high $A_V$ values. The scatter of the $\gamma_{\rm low}$ and $\delta_{\rm low}$ values between clouds is a factor of 2.5 (for $\gamma$) and 4.5 (for $\delta$) larger than for the high extinction regions. Essentially this paints the following picture of the cloud structure: The low $A_V$ and turbulence dominated regions differ from cloud to cloud. Their column density and mass distributions are determined by the environment of the cloud and the feedback they have experienced from the star formation processes within them. Above a (column) density threshold of about 6 mag $A_V$, which is independent of the cloud, gravity becomes the dominant force in shaping the structure. This part of the cloud is then more and more decoupled from the influences of its surrounding turbulent field, and thus the column density and mass distributions for all clouds are virtually identical above the extinction threshold. This also implies that local feedback from young clusters or stars has no significant influence in shaping the column density and mass distributions.

**ACKNOWLEDGEMENTS**

JR acknowledges a University of Kent scholarship. This publication makes use of data products from the Two Micron All Sky Survey, which is a joint project of the University of Massachusetts and the Infrared Processing and Analysis Center/California Institute of Technology, funded by the National Aeronautics and Space Administration and the National Science Foundation.

**REFERENCES**

Alves, J., Lombardi, M., Lada, C. J. 2007, A&A, 462, 17
Ballesteros-Paredes, J., Hartmann, L., Vázquez-Semadeni, E. 1999, ApJ, 527, 285
Bally, J., Reipurth, B., Lada, C. J., Billawala, Y. 1999, AJ, 117, 410
Boldyrev, S. 2002, ApJ, 569, 841
Cambrésy, L., 1999, A&A, 345, 965
Carpenter, J. & Hodapp, K. 2008 in HSFR VI, 899
Dobashi, K., Uehara, H., Kandori, R., Sakurai, T., 2005, PASJ, 57, 1
Elmegreen, B. G. & Scalo, J. 2004, A&A, 42, 211
Froebrich, D., del Burgo, C., 2006, MNRAS, 369, 1901
Froebrich, D., Murphy, G. C., Smith, M. D., Walsh, J., del Burgo, C. 2007, MNRAS, 378, 1447
Froebrich, D. & Rowles, J. 2010 Bulletin of the Astronomical Society of India, in press
Glover, S. C. O., Federrath, C., Mac Low, M., 2009 in press
Goodman, A. A., Pineda, J. E., Schnee, S. L. 2008, ApJ, 692, 91
Hartmann, L., Ballesteros-Paredes, J. & Bergin, E.A. 2001, ApJ, 562, 852
Hilditch, R. W., Howarth, I. D., Harries, T. J. 2005, MNRAS, 357, 304
Johnstone, D., Di Francesco, J., Kirk, H. 2004, ApJ, 611, 45
Kainulainen, J., Beuther, H., Henning, T., Plume, R. 2009, A&A, in press
Kenyon, S. J., Gomez, M., Whitney, B. A. 2008, HSFR VI, 405
Klessen, R. S., Heitsch, F., Mac Low, M.-M. 2000, ApJ, 535, 887
Knude, J. & Hog, E. 1998, A&A, 338, 897
Kolmogorov, A. 1941, DoSSR, 30, 301
Kun, M., Kiss, Z. T., Balog, Z. 2008, HSFR VI, 136
Lada, C. J., Lada, E. A., Clemens, D. P., Bally, J 1994, ApJ, 429, 694
Lada, C. J., Lada, E. A. 2003, A&A, 41, 57
Lada, C. J., Lombardi, M., Alves, J. F. 2009, ApJ, 703, 52
Lombardi, M., Lada, C. J., Alves, J. 2008, A&A, 480, 785
Lombardi, M., Lada, C. J., Alves, J. 2008, A&A, 489, 143
Macri, L. M., Stanek, K. Z., Bersier, D., Greenhill, L. J., 2006, ApJ, 652, 1133
Motte, F. & André, P. 2001, A&A, 365, 440
Muench, A., Getman, K., Hillenbrand, L., Preibisch, T. 2008, HSFR VI, 483
Padoan, P., Jones, B. J. T., Nordlund, A. P. 1997, ApJ, 474, 730
Robin, A. C., Reylé, C., Derrière, S., 2003, A&A, 409, 523
Rowles, J. & Froebrich, D. 2009, MNRAS, 395, 1640
Scalo, J. & Elmegreen, B. G. 2004, A&A, 42, 275
Schlegel, D. J., Finkbeiner, D. P., Davis, M. 1998, ApJ, 500, 525
She, Z.-S. & Leveque, E. 1994, PhRvL, 72, 336
Skrutskie, M.F., Cutri, R.M., Stiening, R., Weinberg, M.D., Schneider, S., Carpenter, J.M., Beichman, C., and et al., 2006, AJ, 131, 1163-1183

Straizys, V., Cernis, K., Bartasiue, S. 1996, BaltA, 5, 125
Vázquez-Semadeni, E. & García, N. 2001, ApJ, 557, 727

## APPENDIX A: DEPENDENCE OF $\gamma_{\rm LOW}$ ON SCALE

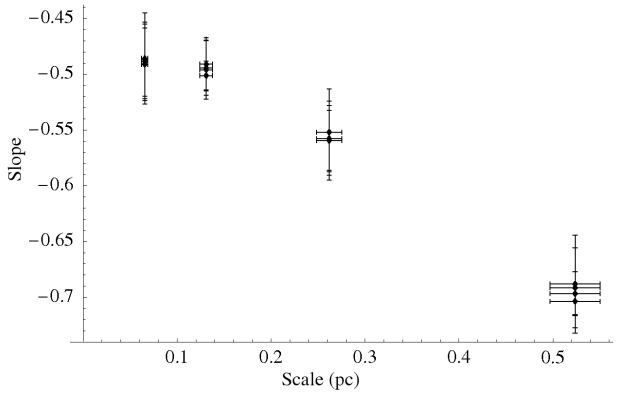


**Figure A1.** Dependence of the slope $\gamma_{\rm low}$ for the cloud Auriga 1 on the spatial scale. Shown are the values for each spatial resolution and histogram bin width.

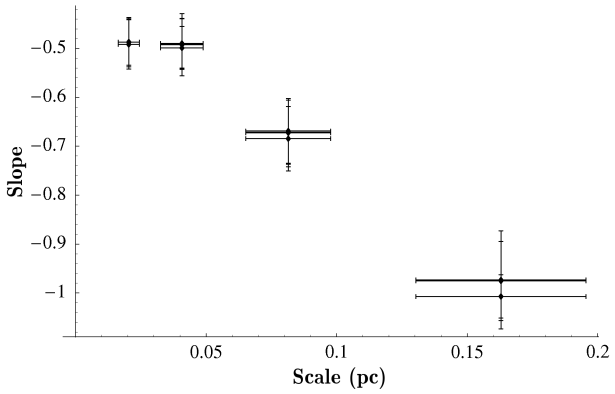


**Figure A2.** As Fig. A1 but for the cloud Auriga 2.

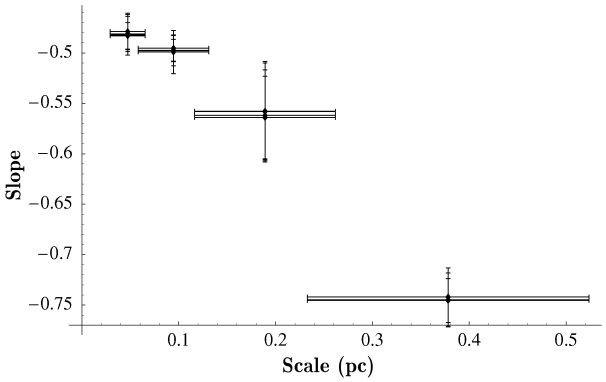


**Figure A3.** As Fig. A1 but for the cloud Cepheus.

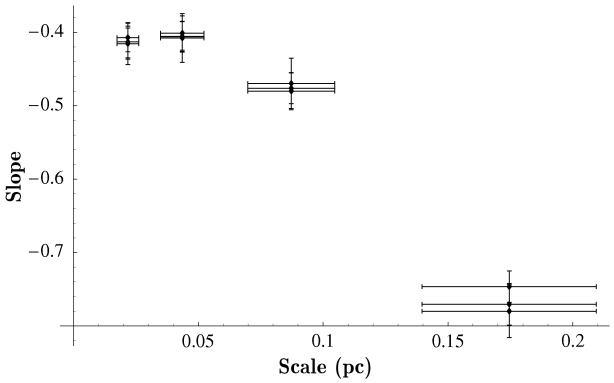


**Figure A4.** As Fig. A1 but for the cloud Chamaeleon.

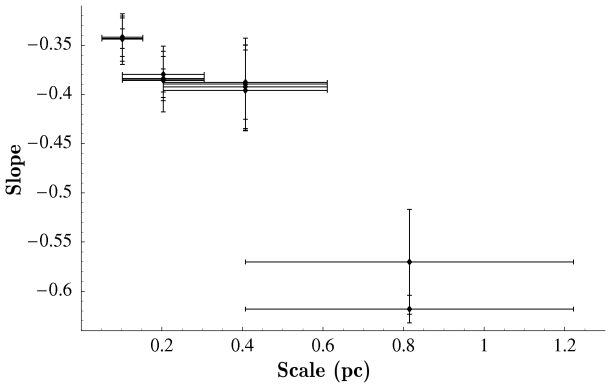


**Figure A5.** As Fig. A1 but for the cloud Circinus.

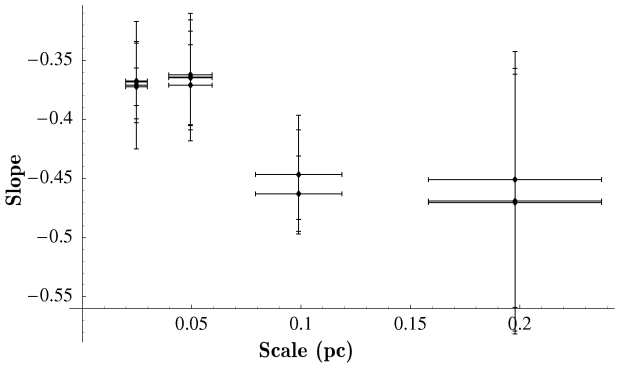


**Figure A6.** As Fig. A1 but for the cloud Corona Australis.

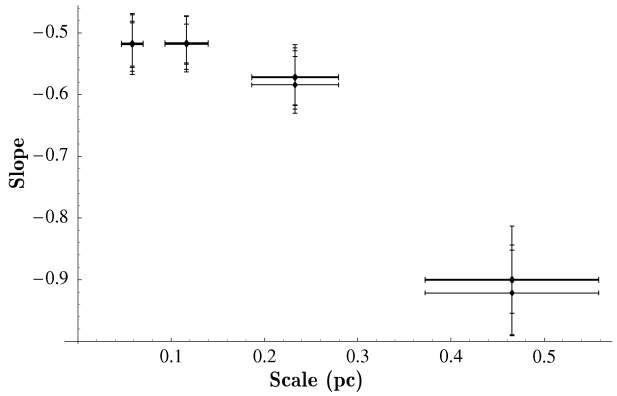


**Figure A7.** As Fig. A1 but for the cloud $\lambda$-Ori.

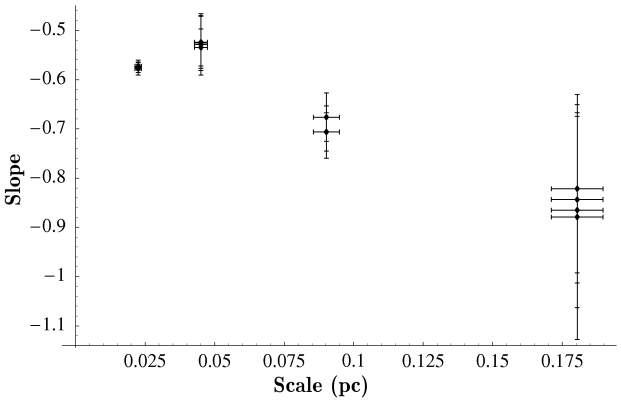


**Figure A8.** As Fig. A1 but for the cloud Lupus 1, 2.

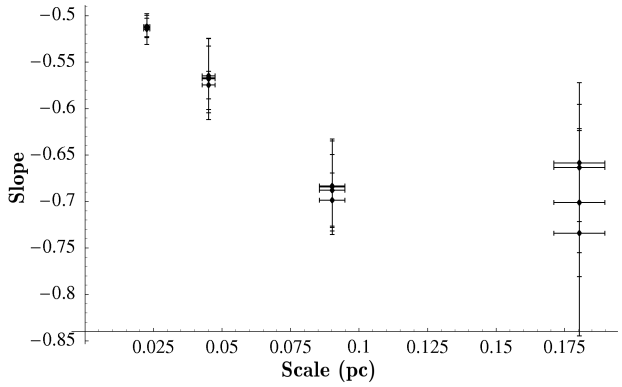


**Figure A9.** As Fig. A1 but for the cloud Lupus 3, 4, 5, 6.

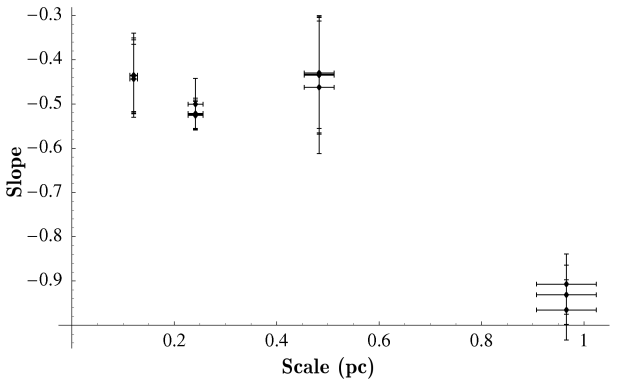


**Figure A10.** As Fig. A1 but for the cloud Monoceros.

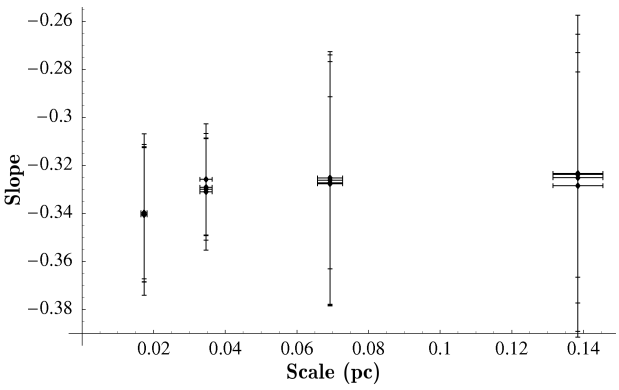


**Figure A11.** As Fig. A1 but for the cloud Ophiuchus.

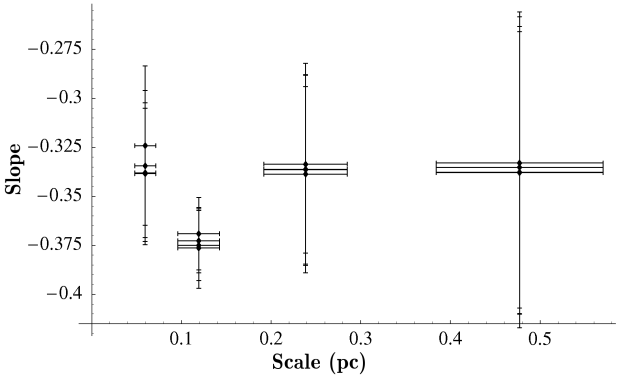


**Figure A12.** As Fig. A1 but for the cloud Orion A.

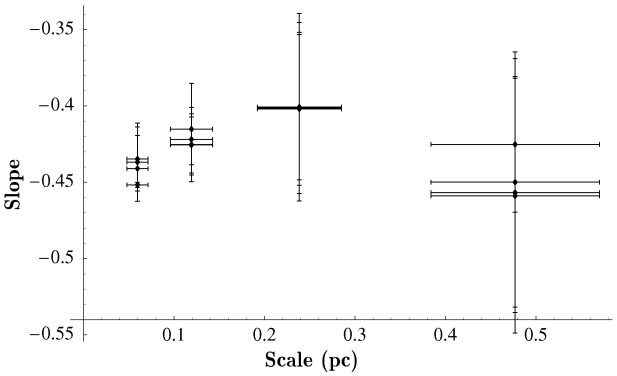


**Figure A13.** As Fig. A1 but for the cloud Orion B.

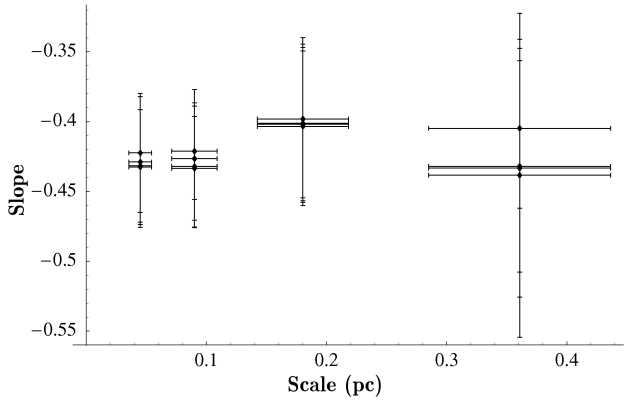


**Figure A14.** As Fig. A1 but for the cloud Perseus.

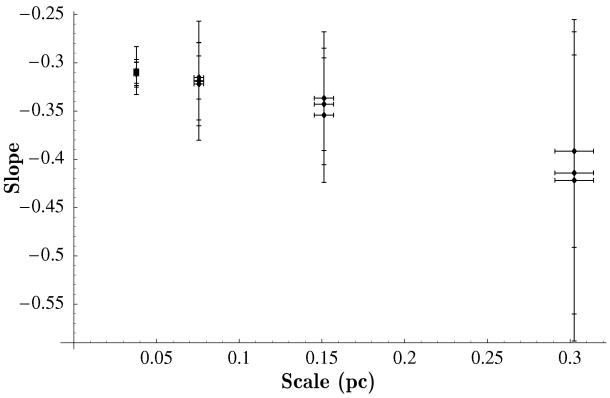


**Figure A15.** As Fig. A1 but for the cloud Serpens.

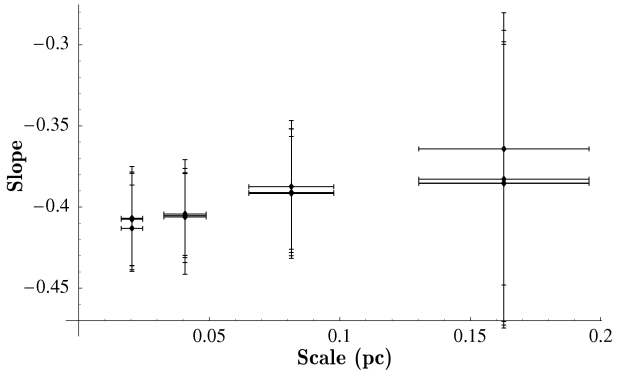


**Figure A16.** As Fig. A1 but for the cloud Taurus.

### A1 Effect of rebinning of data on $\gamma_{\rm low}$

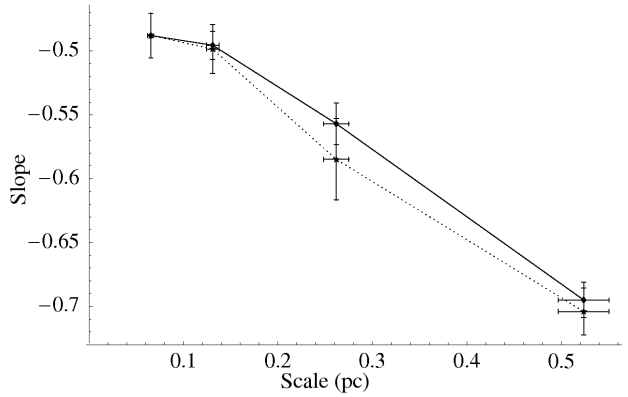


**Figure A17.** Dependence of the slope $\gamma_{\rm low}$ for the cloud Auriga 1 on the spatial scale for the original data (solid line) and when the highest resolution image is rebinned to the lower spatial resolution (dotted line).

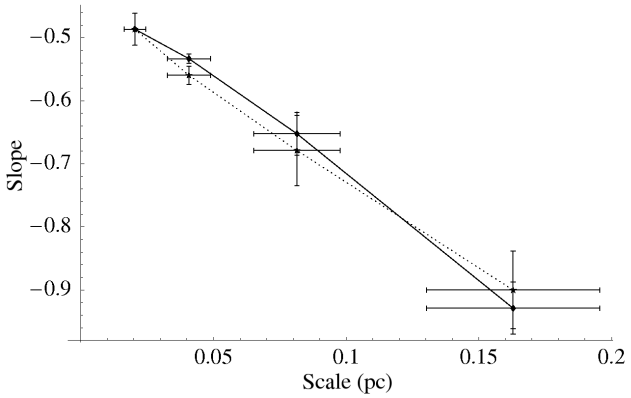


**Figure A18.** As Fig. A17 but for the cloud Auriga 2.

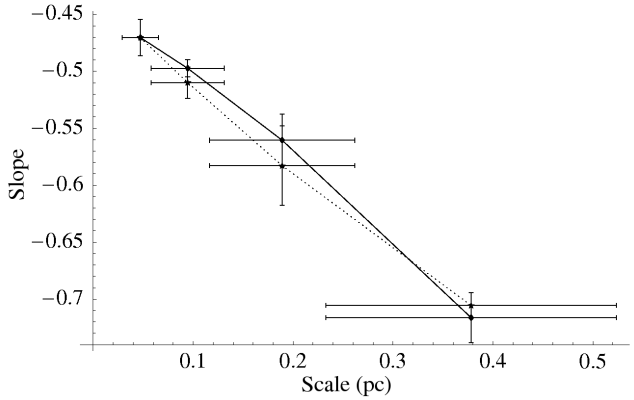


**Figure A19.** As Fig. A17 but for the cloud Cepheus.

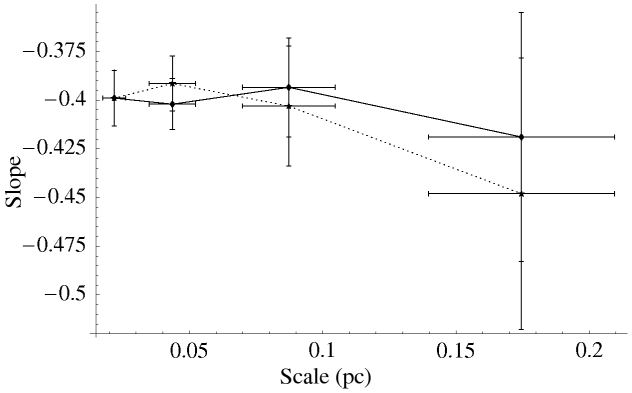


**Figure A20.** As Fig. A17 but for the cloud Chamaeleon.

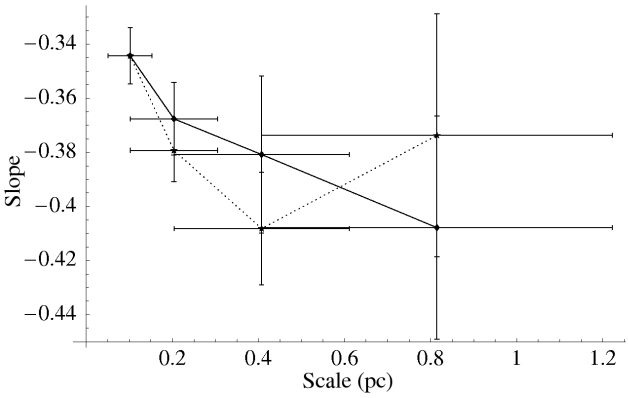


**Figure A21.** As Fig. A17 but for the cloud Circinus.

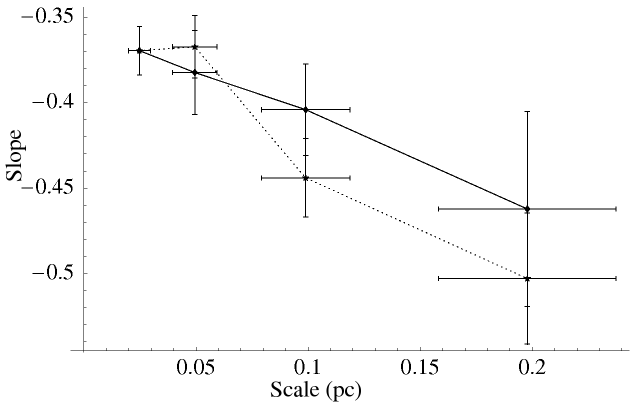


**Figure A22.** As Fig. A17 but for the cloud Corona Australis.

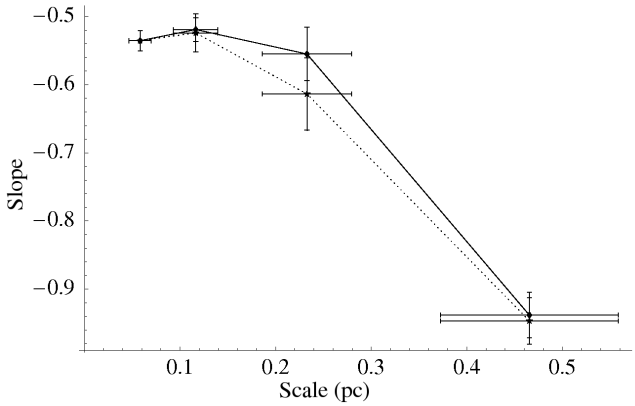


**Figure A23.** As Fig. A17 but for the cloud $\lambda$-Ori.

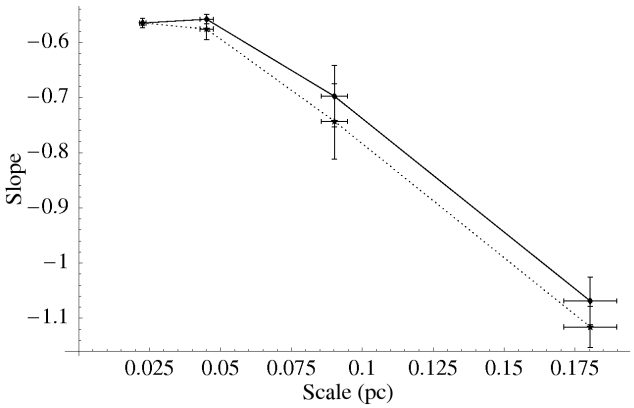


**Figure A24.** As Fig. A17 but for the cloud Lupus 1, 2.

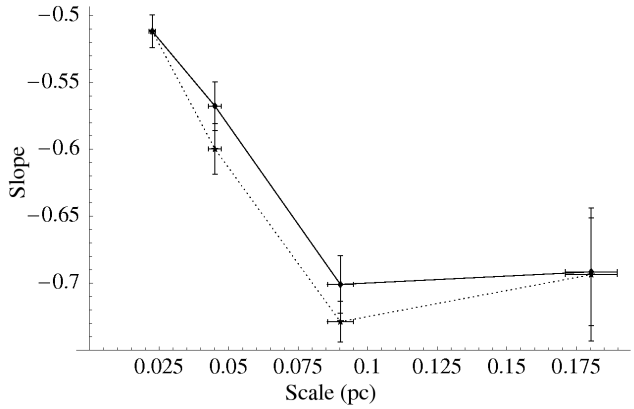


**Figure A25.** As Fig. A17 but for the cloud Lupus 3, 4, 5, 6.

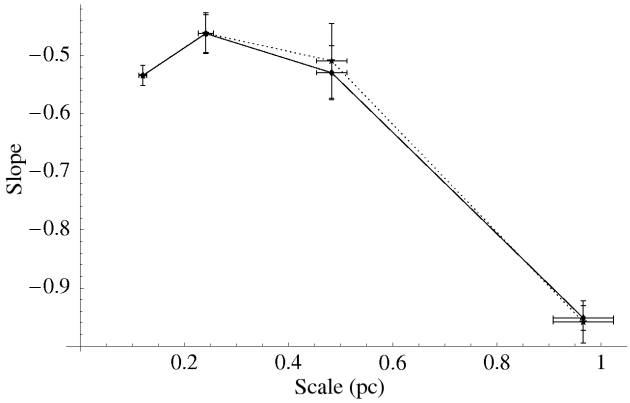


**Figure A26.** As Fig. A17 but for the cloud Monoceros.

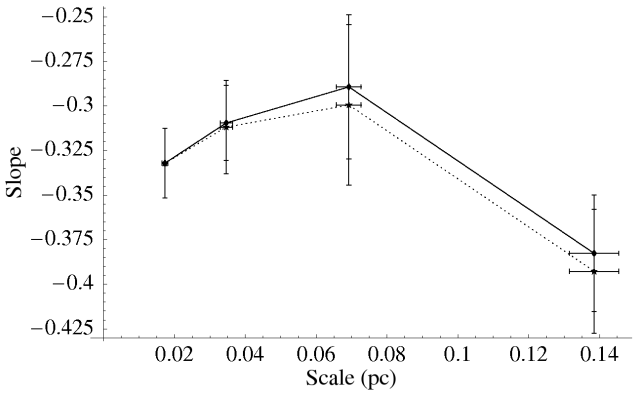


**Figure A27.** As Fig. A17 but for the cloud Ophiuchus.

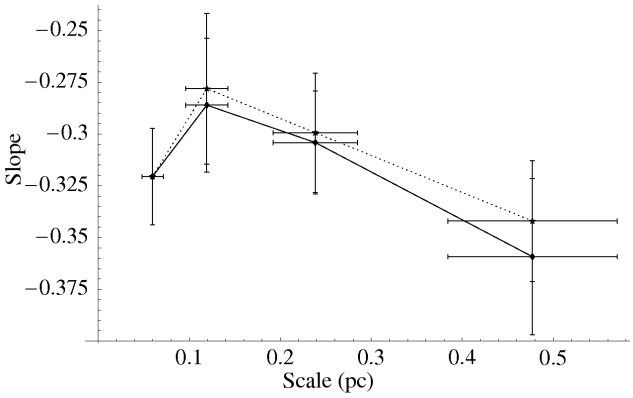


**Figure A28.** As Fig. A17 but for the cloud Orion A.

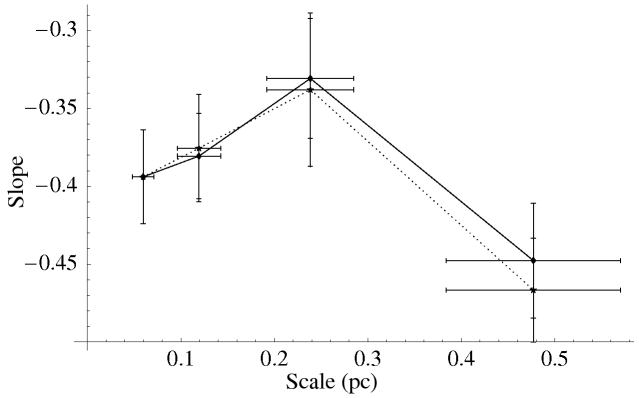


**Figure A29.** As Fig. A17 but for the cloud Orion B.

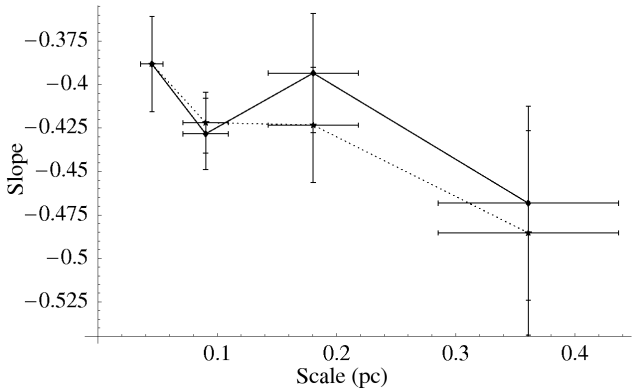


**Figure A30.** As Fig. A17 but for the cloud Perseus.

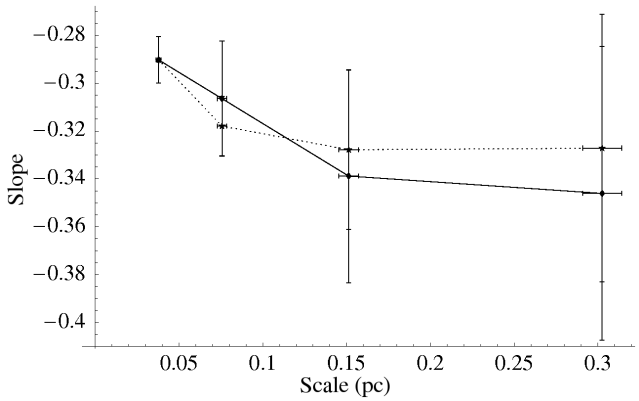


**Figure A31.** As Fig. A17 but for the cloud Serpens.

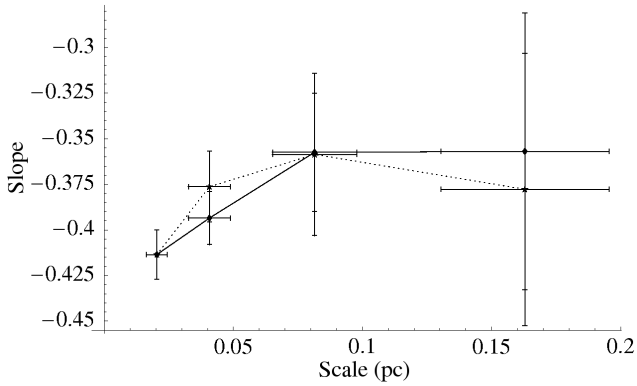


**Figure A32.** As Fig. A17 but for the cloud Taurus.

### A2 Effect of rebinning of data on $\gamma_{\rm high}$

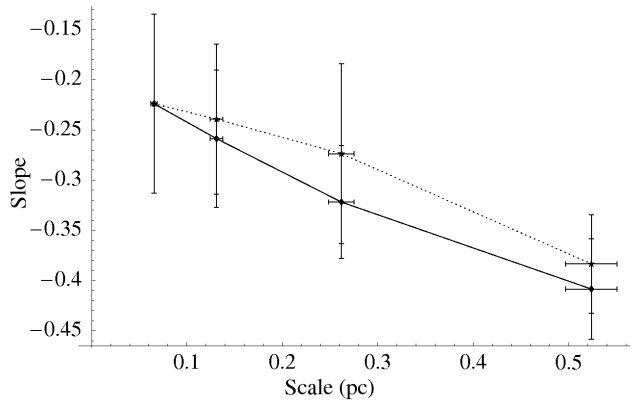


**Figure A33.** Dependence of the slope $\gamma_{\rm high}$ for the cloud Auriga 1 on the spatial scale for the original data (solid line) and when the highest resolution image is rebinned to the lower spatial resolution (dotted line).

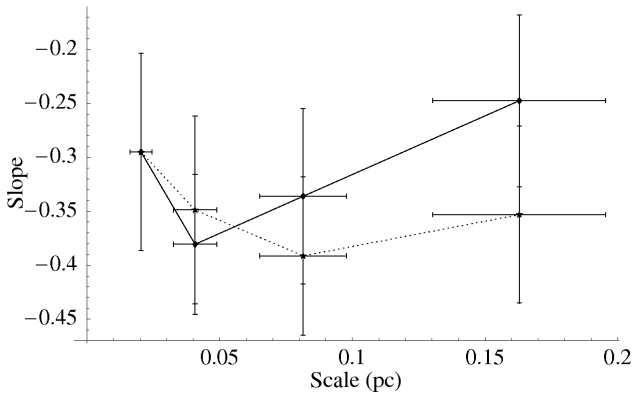


**Figure A34.** As Fig. A33 but for the cloud Auriga 2.

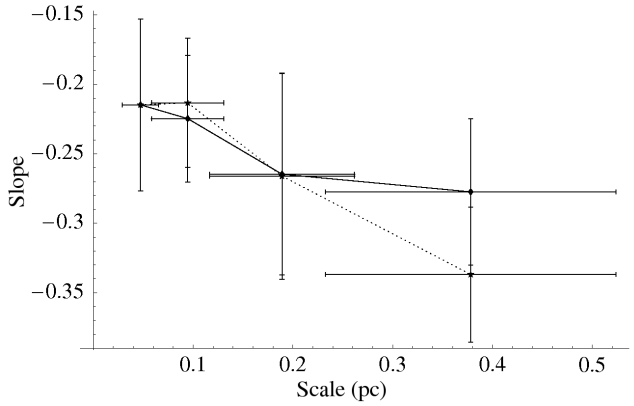


**Figure A35.** As Fig. A33 but for the cloud Cepheus.

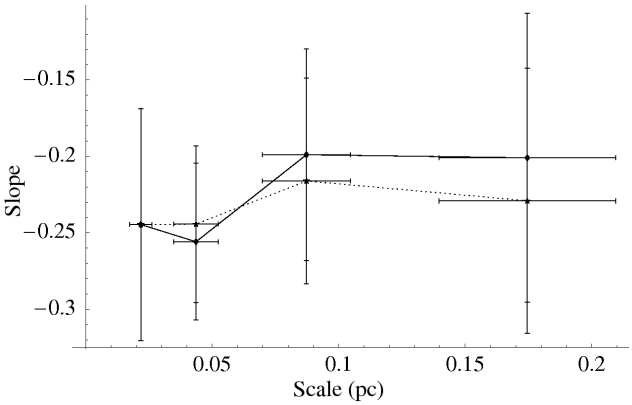


**Figure A36.** As Fig. A33 but for the cloud Chamaeleon.

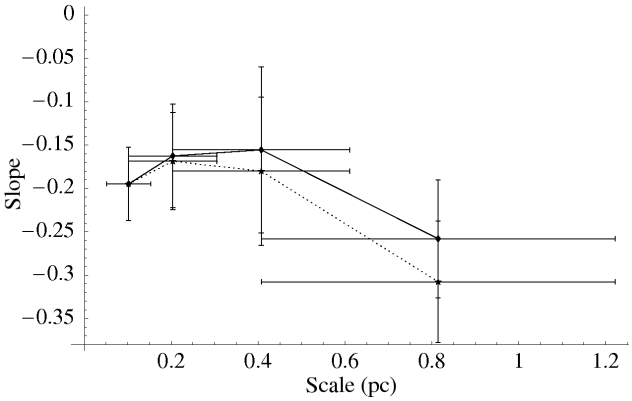


**Figure A37.** As Fig. A33 but for the cloud Circinus.

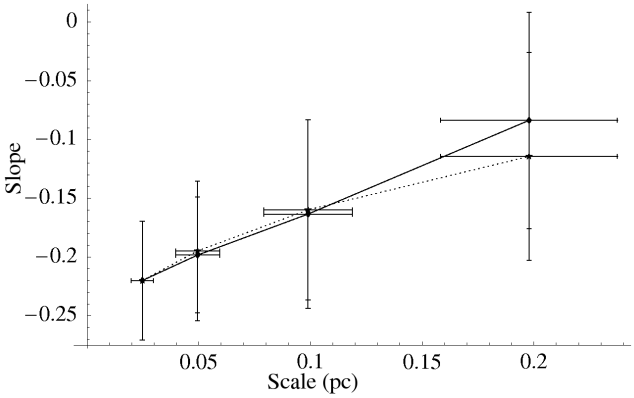


**Figure A38.** As Fig. A33 but for the cloud Corona Australis.

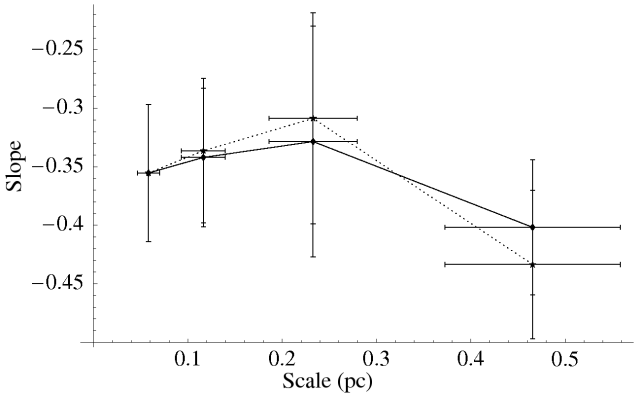


**Figure A39.** As Fig. A33 but for the cloud $\lambda$-Ori.

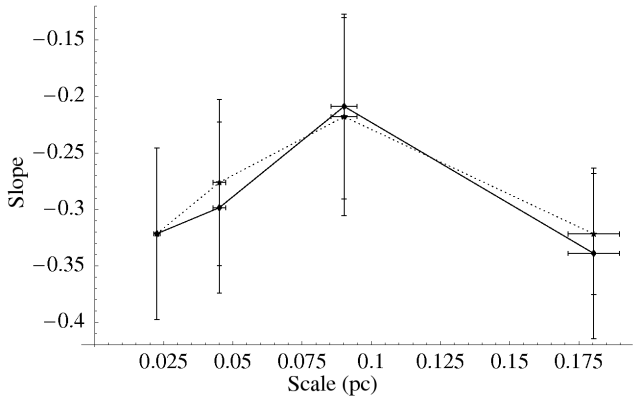


**Figure A40.** As Fig. A33 but for the cloud Lupus 1, 2.

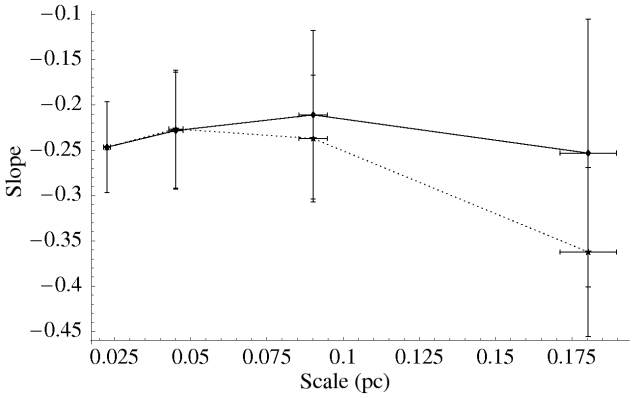


**Figure A41.** As Fig. A33 but for the cloud Lupus 3, 4, 5, 6.

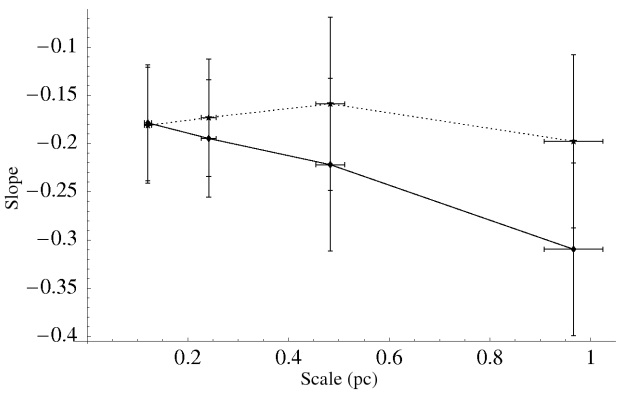


**Figure A42.** As Fig. A33 but for the cloud Monoceros.

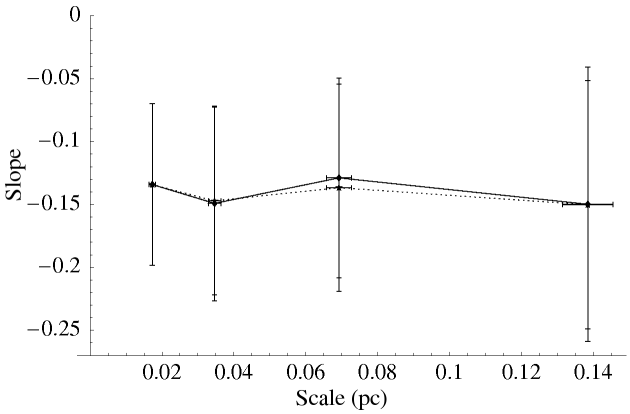


**Figure A43.** As Fig. A33 but for the cloud Ophiuchus.

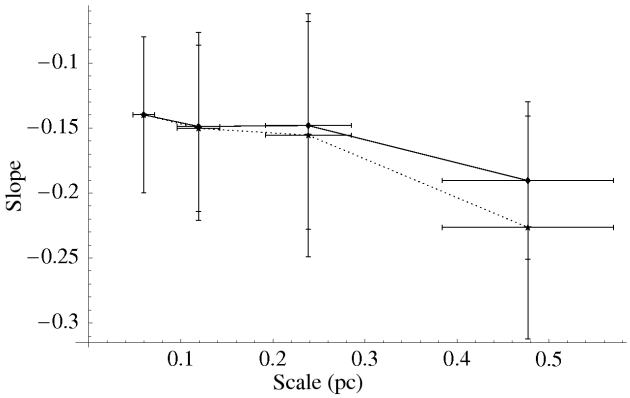


**Figure A44.** As Fig. A33 but for the cloud Orion A.

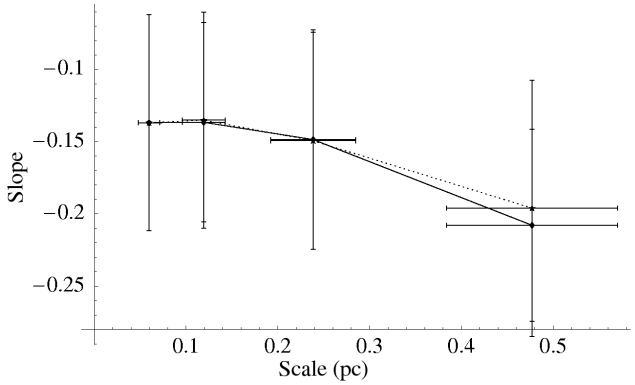


**Figure A45.** As Fig. A33 but for the cloud Orion B.

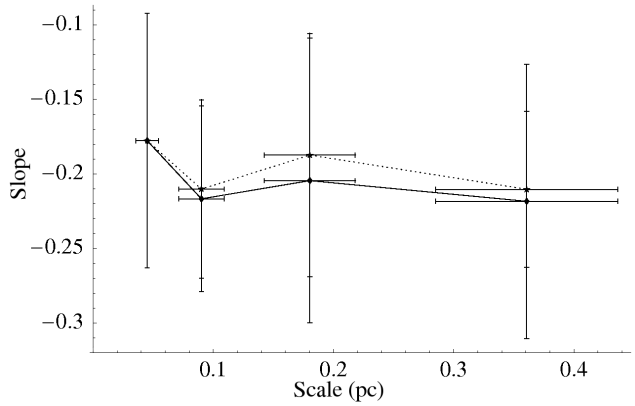


**Figure A46.** As Fig. A33 but for the cloud Perseus.

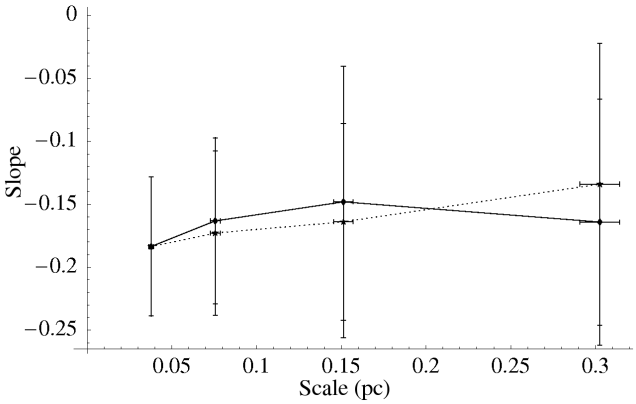


**Figure A47.** As Fig. A33 but for the cloud Serpens.

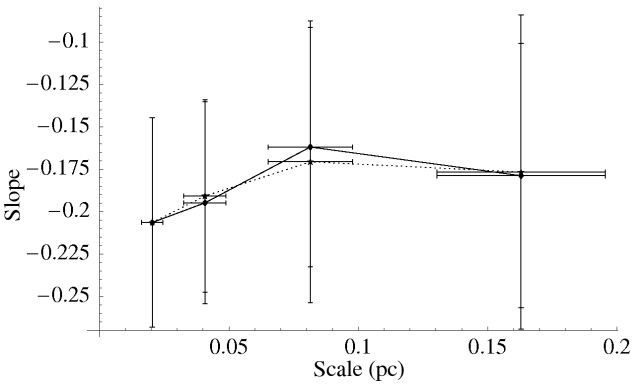


**Figure A48.** As Fig. A33 but for the cloud Taurus.

### A3 Log-normal fits to the normalised Column Density Distributions

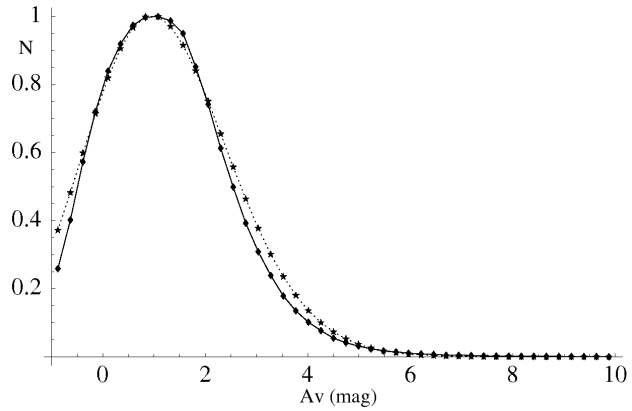


**Figure A49.** Best log-normal fit (dotted line) to the Column Density Distribution for the cloud Auriga 1 (solid line) for a spatial scale of 0.1 pc.

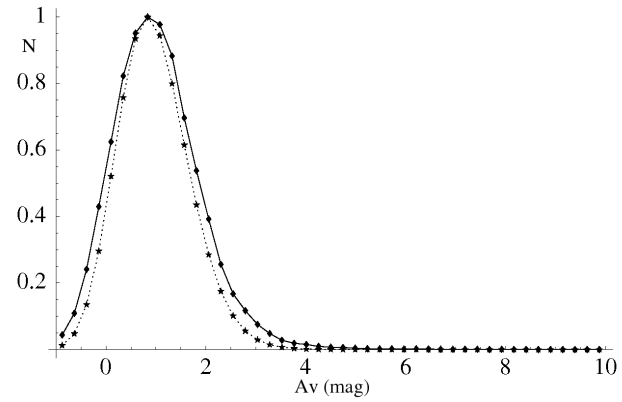


**Figure A50.** As Fig. A49 but for the cloud Auriga 2.

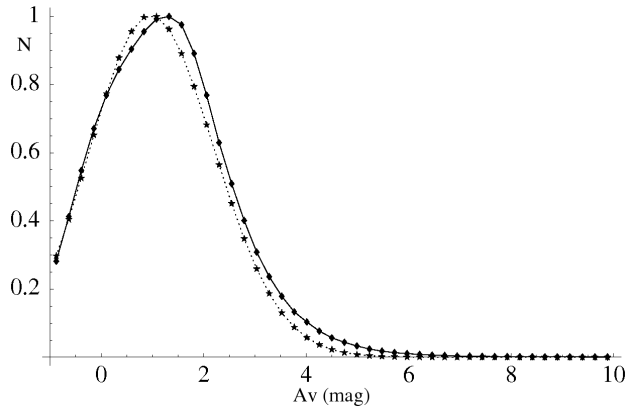


**Figure A51.** As Fig. A49 but for the cloud Cepheus.

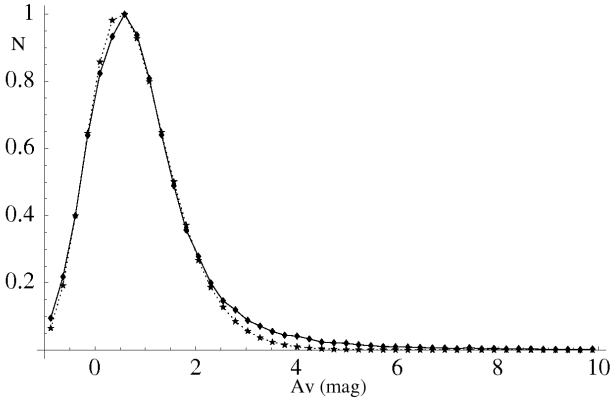


**Figure A52.** As Fig. A49 but for the cloud Chamaeleon.

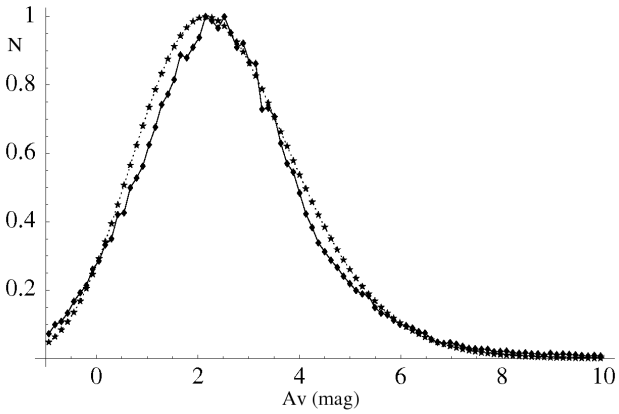


**Figure A53.** As Fig. A49 but for the cloud Circinus.

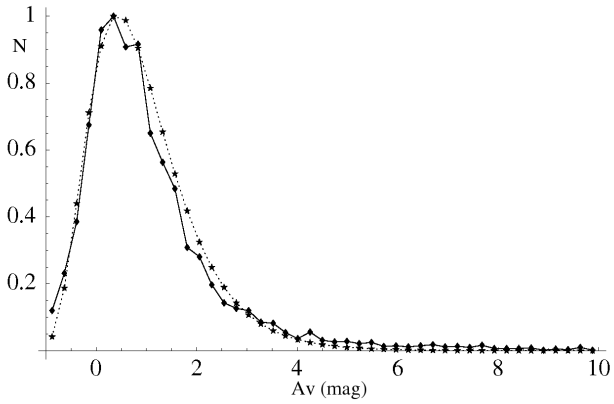


**Figure A54.** As Fig. A49 but for the cloud Corona Australis.

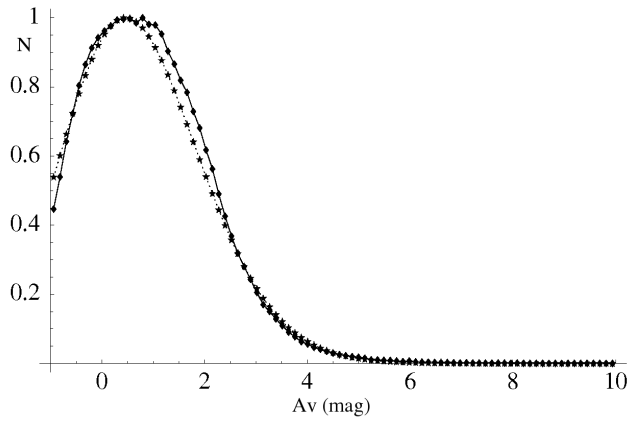


**Figure A55.** As Fig. A49 but for the cloud $\lambda$-Ori.

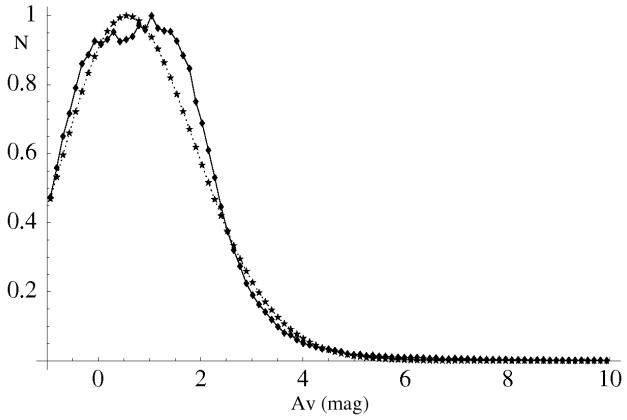


**Figure A58.** As Fig. A49 but for the cloud Monoceros.

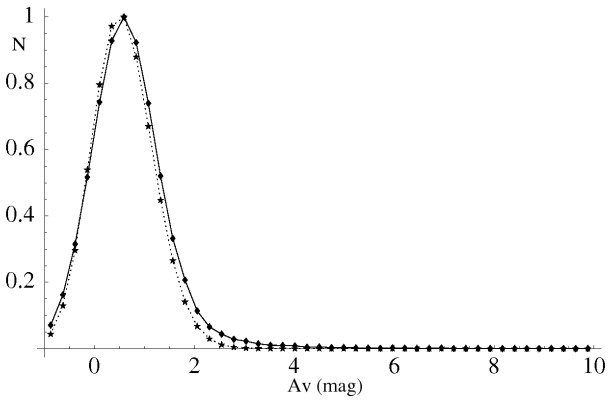


**Figure A56.** As Fig. A49 but for the cloud Lupus 1, 2.

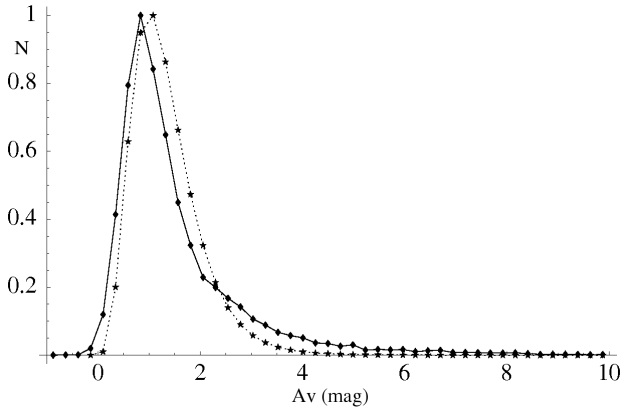


**Figure A59.** As Fig. A49 but for the cloud Ophiuchus.

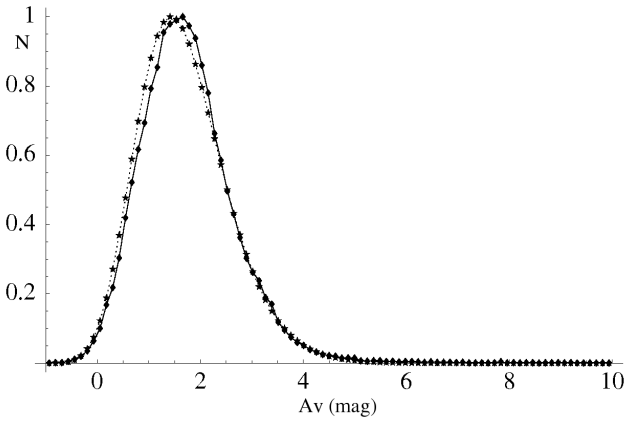


**Figure A57.** As Fig. A49 but for the cloud Lupus 3, 4, 5, 6.

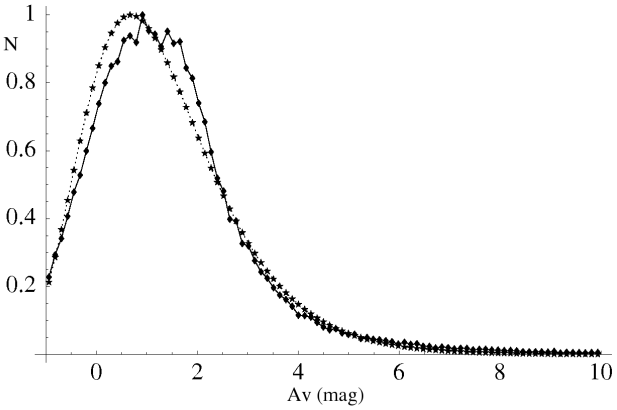


**Figure A60.** As Fig. A49 but for the cloud Orion A.

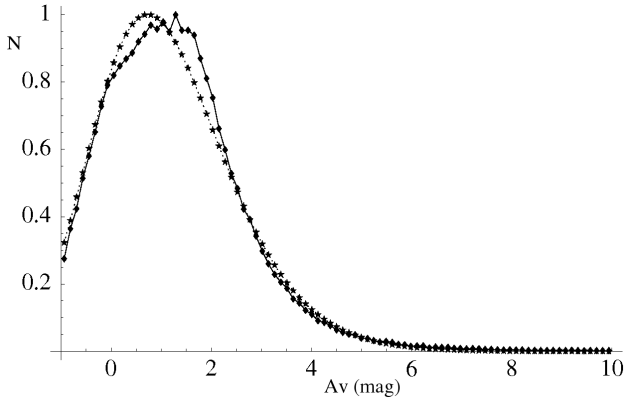


**Figure A61.** As Fig. A49 but for the cloud Orion B.

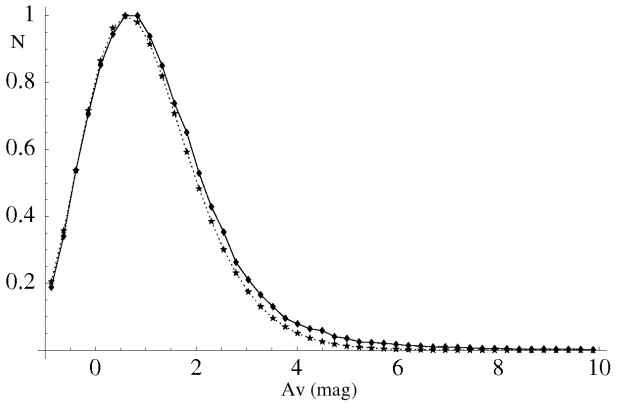


**Figure A64.** As Fig. A49 but for the cloud Taurus.

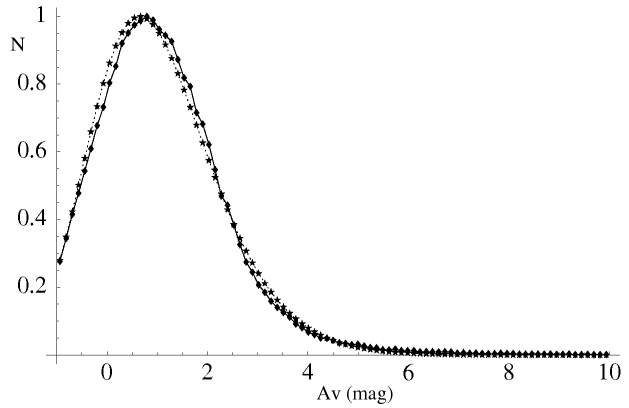


**Figure A62.** As Fig. A49 but for the cloud Perseus.

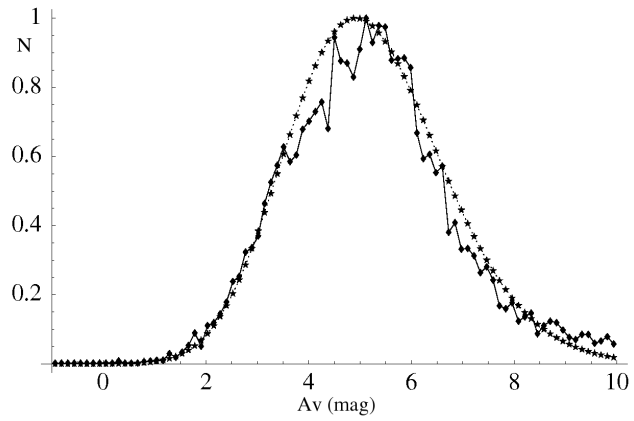


**Figure A63.** As Fig. A49 but for the cloud Serpens.

### A4 The log(N) vs $A_V$ Column Density Distributions

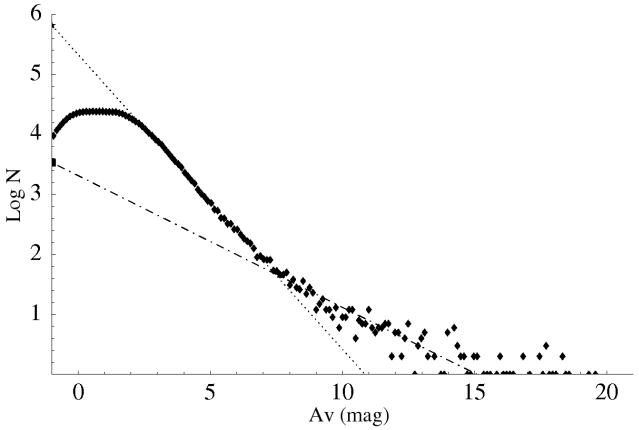


**Figure A65.** Best fits (dotted line) to the Column Density Distribution for the cloud Auriga 1 (solid line) for a spatial scale of 0.1 pc. Both fits (for the high and low column density regions) are shown.

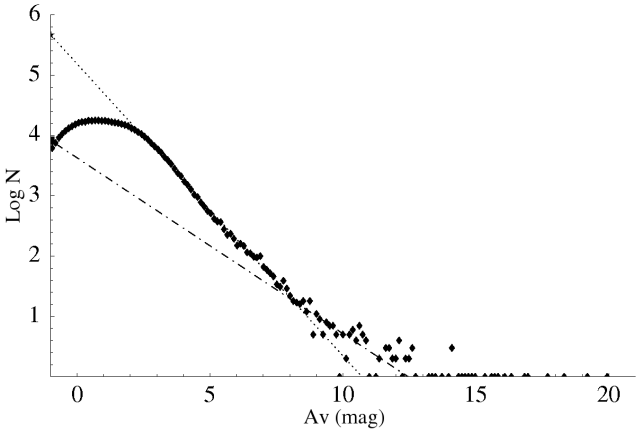


**Figure A66.** As Fig. A65 but for the cloud Auriga 2.

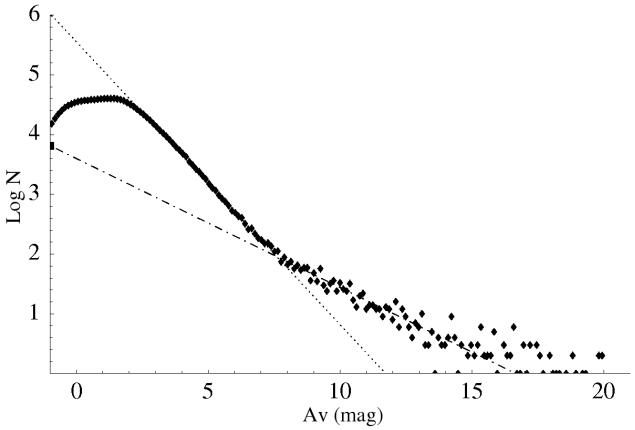


**Figure A67.** As Fig. A65 but for the cloud Cepheus.

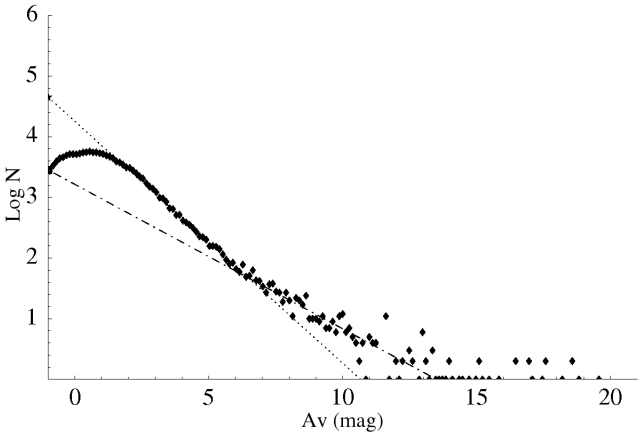


**Figure A68.** As Fig. A65 but for the cloud Chamaeleon.

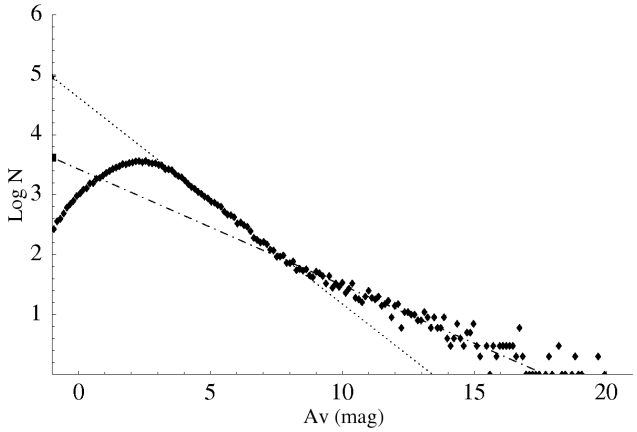


**Figure A69.** As Fig. A65 but for the cloud Circinus.

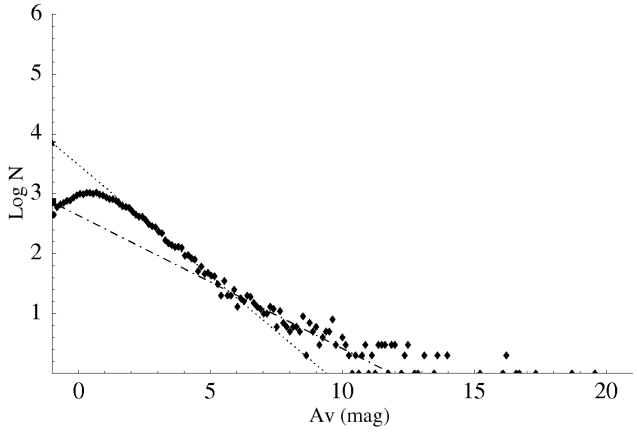


**Figure A70.** As Fig. A65 but for the cloud Corona Australis.

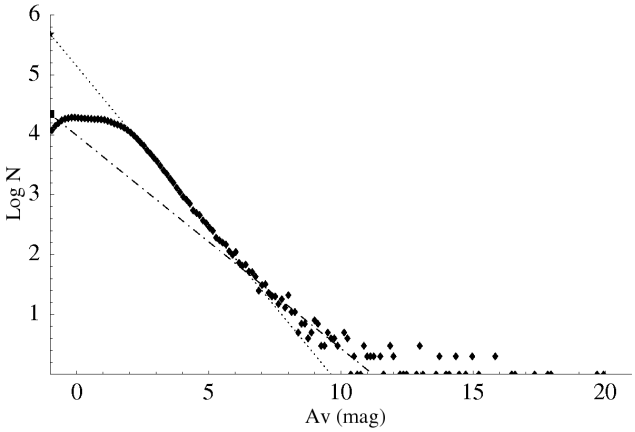


**Figure A71.** As Fig. A65 but for the cloud $\lambda$-Ori.

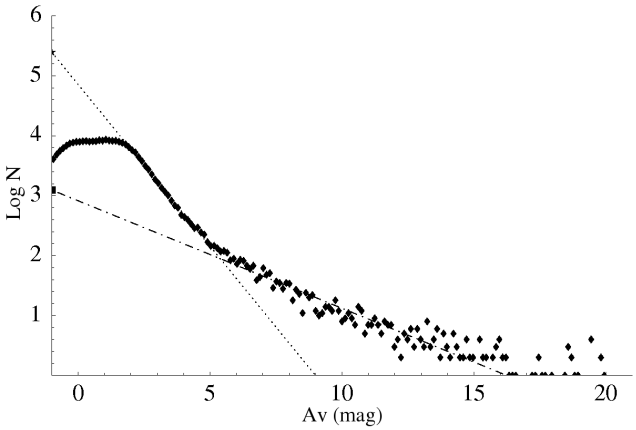


**Figure A74.** As Fig. A65 but for the cloud Monoceros.

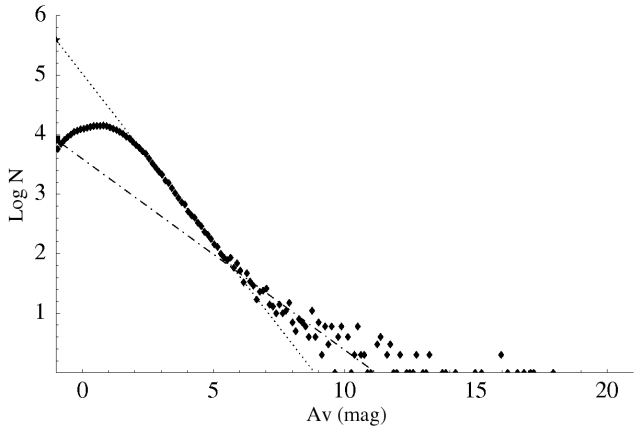


**Figure A72.** As Fig. A65 but for the cloud Lupus 1, 2.

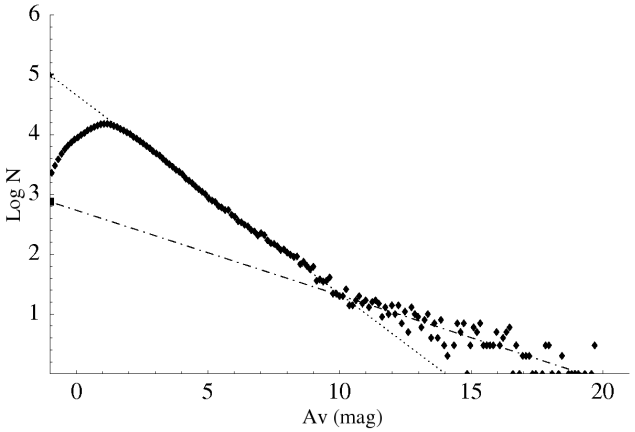


**Figure A75.** As Fig. A65 but for the cloud Ophiuchus.

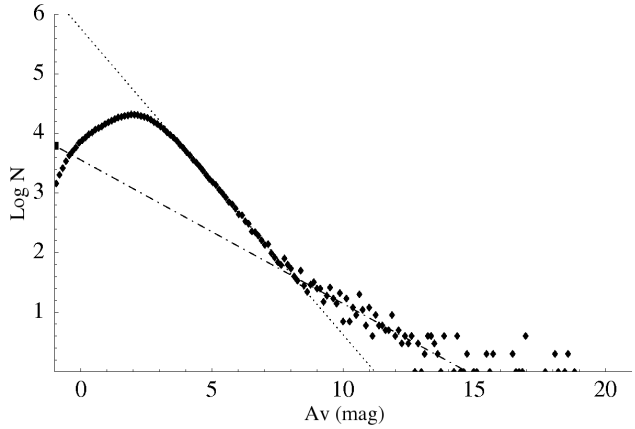


**Figure A73.** As Fig. A65 but for the cloud Lupus 3, 4, 5, 6.

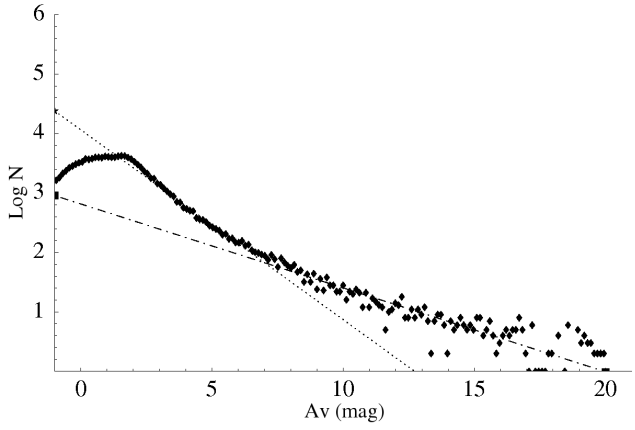


**Figure A76.** As Fig. A65 but for the cloud Orion A.

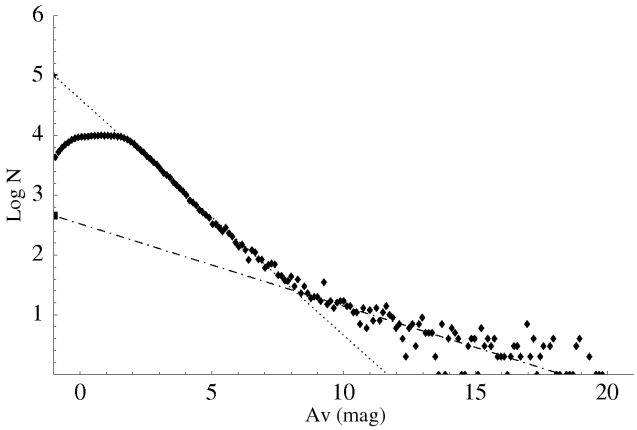


**Figure A77.** As Fig. A65 but for the cloud Orion B.

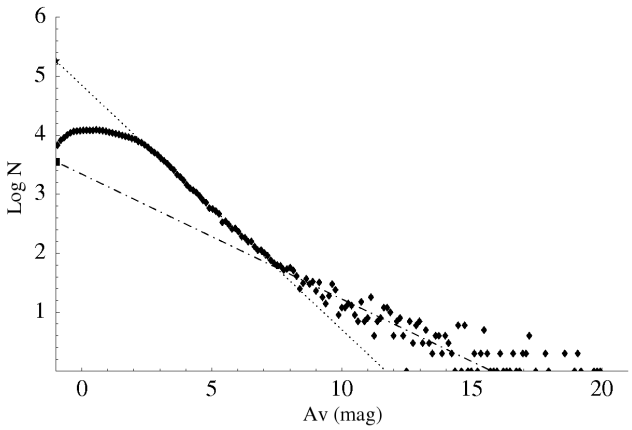


**Figure A80.** As Fig. A65 but for the cloud Taurus.

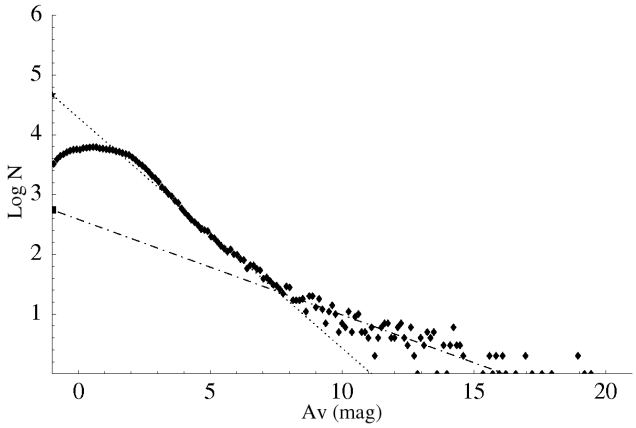


**Figure A78.** As Fig. A65 but for the cloud Perseus.

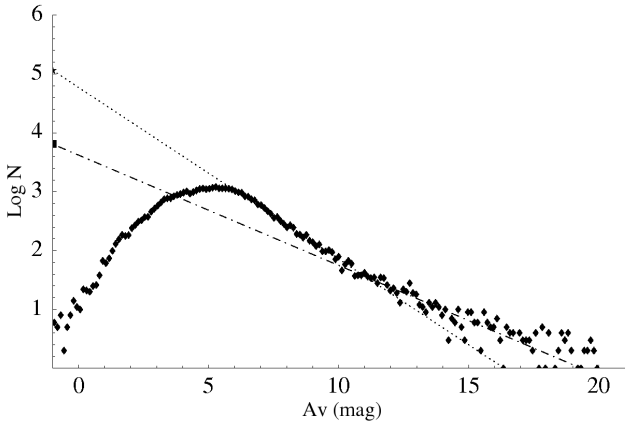


**Figure A79.** As Fig. A65 but for the cloud Serpens.

### A5 The log(M) vs $A_V$ Mass Distributions

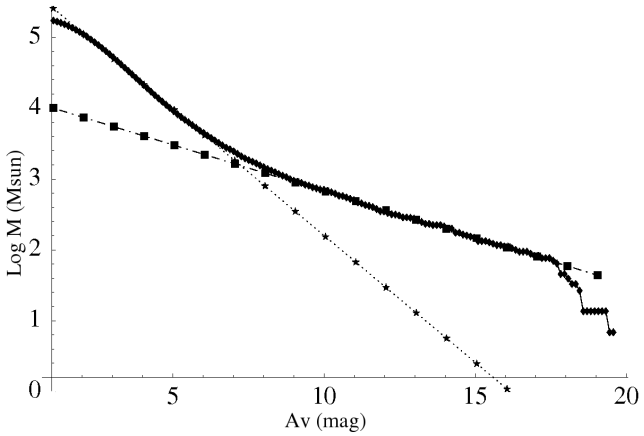


**Figure A81.** Best fits (dotted line) to the Mass Distribution for the cloud Auriga 1 (solid line) for a spatial scale of 0.1 pc. Both fits (for the high and low column density regions) are shown.

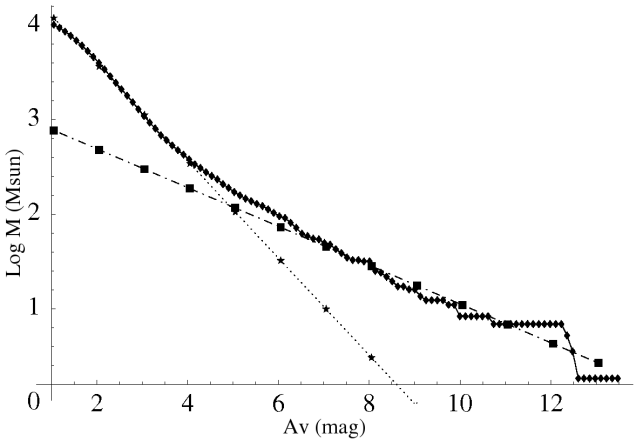


**Figure A82.** As Fig. A81 but for the cloud Auriga 2.

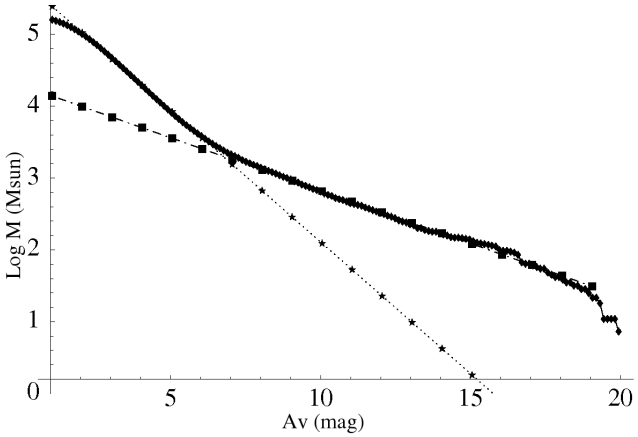


**Figure A83.** As Fig. A81 but for the cloud Cepheus.

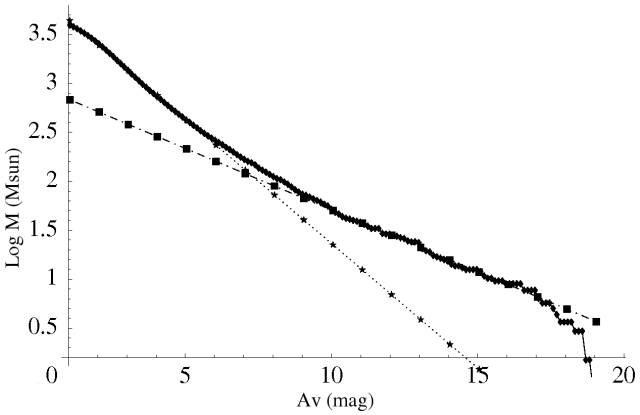


**Figure A84.** As Fig. A81 but for the cloud Chamaeleon.

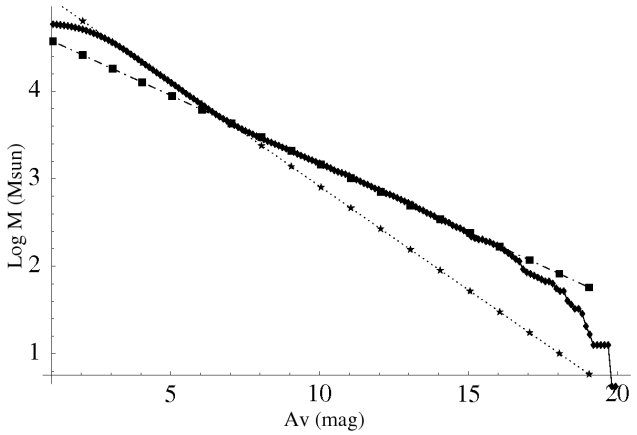


**Figure A85.** As Fig. A81 but for the cloud Circinus.

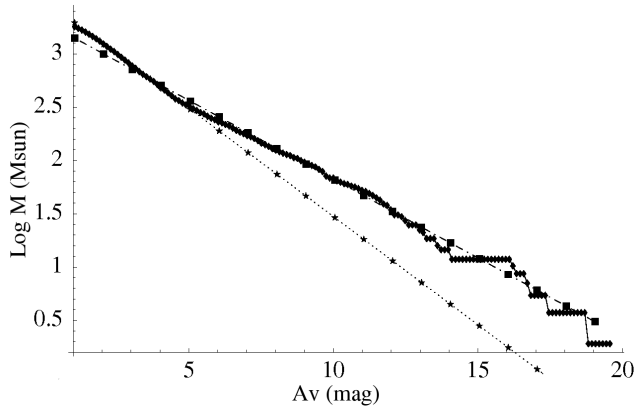


**Figure A86.** As Fig. A81 but for the cloud Corona Australis.

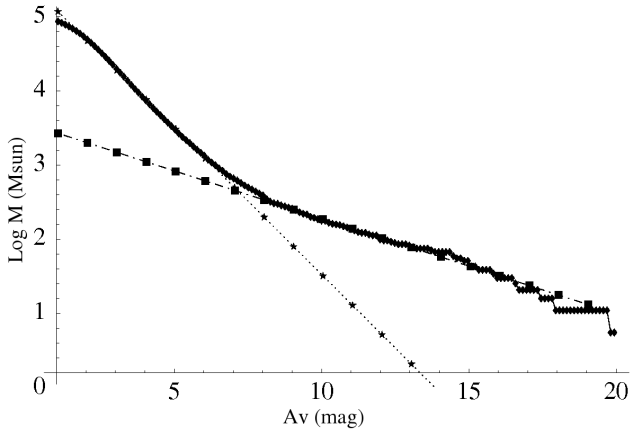


**Figure A87.** As Fig. A81 but for the cloud $\lambda$-Ori.

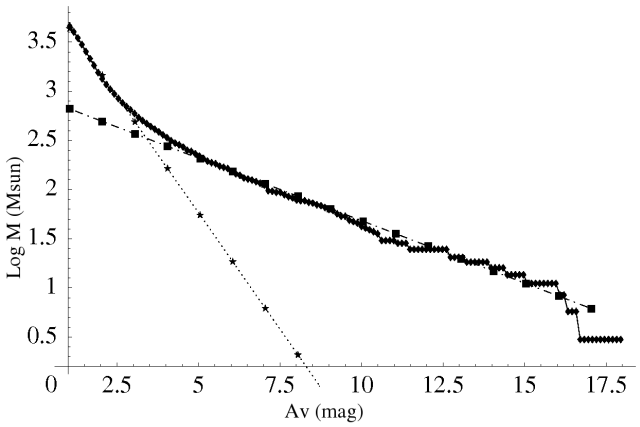


**Figure A88.** As Fig. A81 but for the cloud Lupus 1, 2.

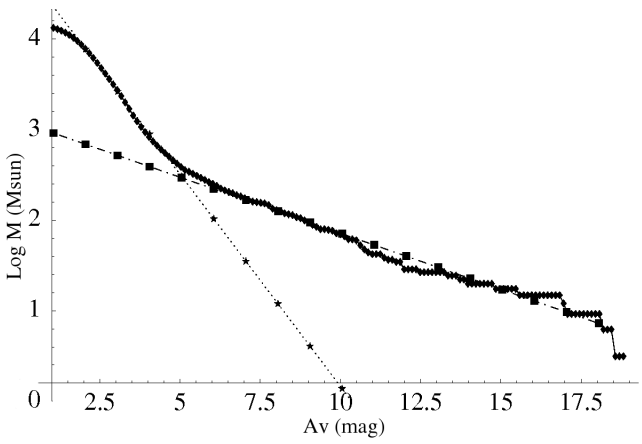


**Figure A89.** As Fig. A81 but for the cloud Lupus 3, 4, 5, 6.

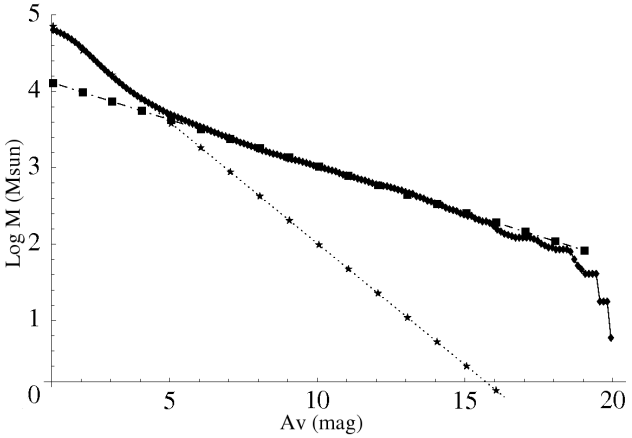


**Figure A90.** As Fig. A81 but for the cloud Monoceros.

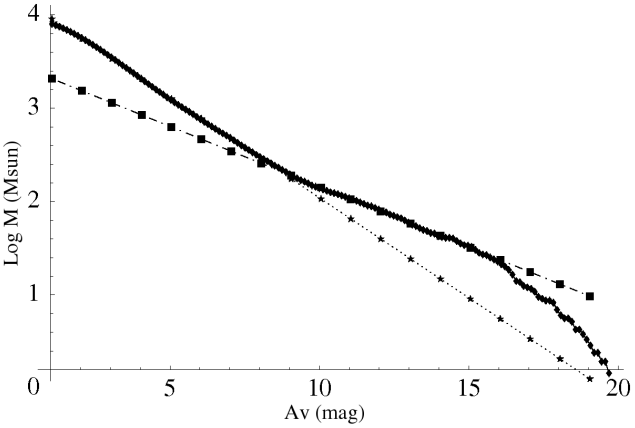


**Figure A91.** As Fig. A81 but for the cloud Ophiuchus.

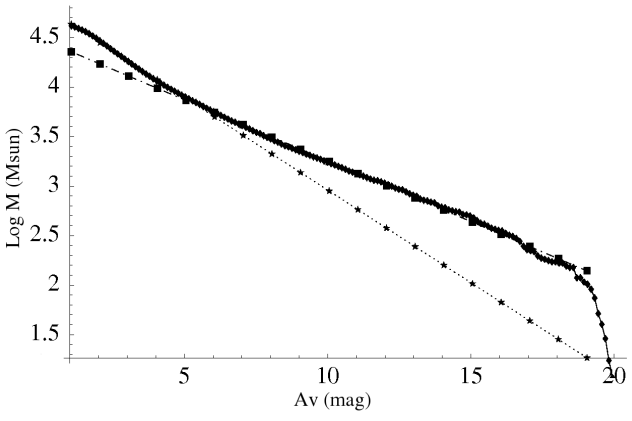


**Figure A92.** As Fig. A81 but for the cloud Orion A.

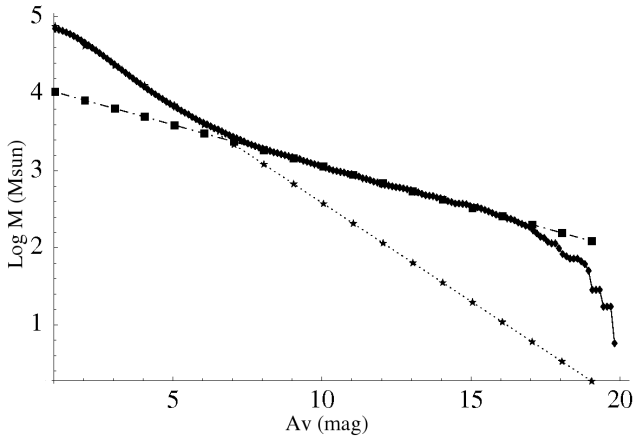


**Figure A93.** As Fig. A81 but for the cloud Orion B.

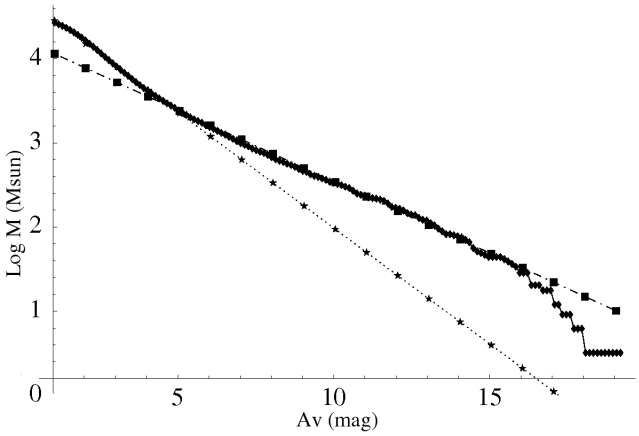


**Figure A94.** As Fig. A81 but for the cloud Perseus.

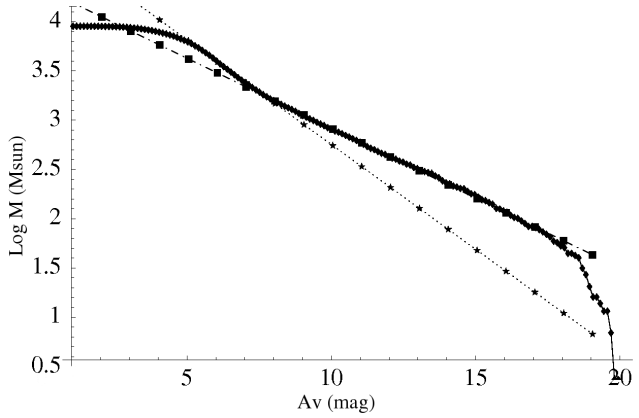


**Figure A95.** As Fig. A81 but for the cloud Serpens.

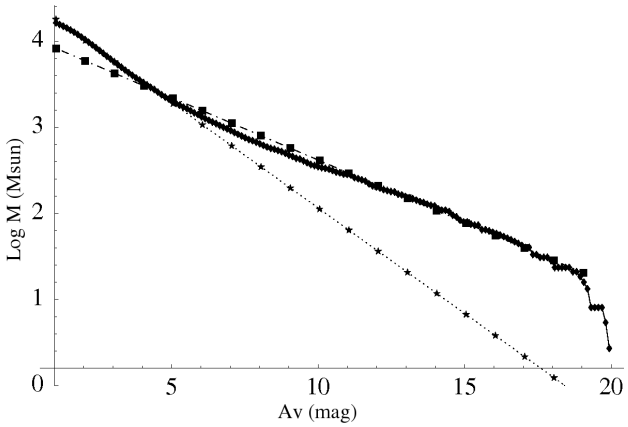


**Figure A96.** As Fig. A81 but for the cloud Taurus.